

ESR/U-series and ESR dating of several Middle Pleistocene Italian sites: Comparison with $^{40}\text{Ar}/^{39}\text{Ar}$ chronology

Original

ESR/U-series and ESR dating of several Middle Pleistocene Italian sites: Comparison with $^{40}\text{Ar}/^{39}\text{Ar}$ chronology / Bahain, J. -J.; Voinchet, P.; Vietti, A.; Shao, Q.; Tombret, O.; Pereira, A.; Nomade, S.; Falgueres, C.. - In: QUATERNARY GEOCHRONOLOGY. - ISSN 1871-1014. - ELETTRONICO. - 63:(2021), p. 101151. [10.1016/j.quageo.2021.101151]

Availability:

This version is available at: 11583/2928512 since: 2021-10-01T10:34:24Z

Publisher:

Elsevier B.V.

Published

DOI:10.1016/j.quageo.2021.101151

Terms of use:

This article is made available under terms and conditions as specified in the corresponding bibliographic description in the repository

Publisher copyright

Elsevier postprint/Author's Accepted Manuscript

© 2021. This manuscript version is made available under the CC-BY-NC-ND 4.0 license
<http://creativecommons.org/licenses/by-nc-nd/4.0/>. The final authenticated version is available online at:
<http://dx.doi.org/10.1016/j.quageo.2021.101151>

(Article begins on next page)

ESR/U-series and ESR dating of several Middle Pleistocene Italian sites: comparison with $^{40}\text{Ar}/^{39}\text{Ar}$ chronology

Jean-Jacques BAHAIN ^{1*}, Pierre VOINCHET ¹, Amina VIETTI ^{1,2}, Qingfeng SHAO ³, Olivier TOMBRET ¹,

Alison PEREIRA ^{1,4,5,6*}, Sébastien NOMADE ⁴, Christophe FALGUÈRES ¹

¹UMR 7194 HNHP Histoire naturelle de l'Homme préhistorique, MNHN-CNRS-UPVD, Département Homme et Environnement du Muséum national d'Histoire naturelle, Institut de Paléontologie Humaine, 1 rue René Panhard, 75013, Paris France

²Dipartimento di chimica, Università degli Studi di Torino, 10125 Turin, Italy

³College of Geographical Science, Nanjing Normal University, Nanjing 210023, China

⁴Laboratoire des Sciences du Climat et de l'Environnement, LSCE/IPSL, CEA-CNRS-UVSQ, Université Paris-Saclay, F-91191 Gif-sur-Yvette, France

⁵Ecole française de Rome, Piazza Farnese, IT-00186, Roma, Italy

⁶Sezione di Scienze Preistoriche e Antropologiche, Dipartimento di Studi Umanistici, Università degli Studi di Ferrara, C.so Ercole d'Este I, 32, Ferrara, Italy

* present adress : UMR 8148 GEOPS Laboratoire Géosciences Paris-Sud, Université Paris-Saclay-CNRS, Campus Vallée, Rue du Belvédère, Bâtiment 504, 91400 Orsay, France

Abstract

The stratigraphic sequences of numerous Palaeolithic sites of Central and Southern Italy, very rich in both archaeological and palaeontological remains, have also recorded Pleistocene volcanic events through volcanic ash deposits (tephra). They allow the establishment of an accurate chronological framework by comparing results obtained by $^{40}\text{Ar}/^{39}\text{Ar}$ dating method on single volcanic K-feldspar crystals, with those derived from ESR and ESR/U-series analyses on fluvial bleached quartz and tooth enamel respectively.

Since 2009, these three methods were hence applied on samples of several Middle Pleistocene sites of Central and Southern Italy including both volcanic and archaeological levels (from the west to the east): La Polledrara di Cenanibbio, Isoletta, (Latium), Guado San Nicola, Isernia La Pineta (Molise), Valle Giumentina (Abruzzo) and Venosa Notarchirico (Basilicata).

The obtained results, covering a time range from 350 to 660 ka, prove that such a multi-method approach when possible is essential to constrain the chronology of each site and allow the recognition of the specific limitations due to the lack of quartz for ESR or to complex geochemical histories in teeth rendering difficult the ESR /U-series method.

30 Despite these limitations, the ESR framework is globally in agreement with the $^{40}\text{Ar}/^{39}\text{Ar}$ chronology, while ESR/U-
31 series dates can be underestimated for the oldest sites. In such cases, an isochron approach attests however of the
32 quite good reliability of the palaeodosimetric reconstruction and the observed age underestimation could be related
33 to other factors affecting the ESR age determination.

34 Key-words – ESR/U-series dating, ESR dating, $^{40}\text{Ar}/^{39}\text{Ar}$ dating, Middle Pleistocene, Palaeolithic, Italy

36 **Introduction**

37 The dating of Middle Pleistocene archaeological sites can usually be performed using a relatively restricted number
38 of geochronological methods. The opportunity to use these technics relies on both the considered time range and
39 available datable materials found on these sites. These parameters greatly depend on the geological context and,
40 consequently, the establishment of accurate chronological framework of the Middle Pleistocene human evolutionary
41 scheme is very heterogeneous in terms of precision and accuracy in the various areas of the world. In Western Europe,
42 this framework was mainly built by uranium-series (U-series) dates on speleothems and by palaeodosimetric dating
43 methods such as thermoluminescence (TL) on heated flints, optically stimulated luminescence (OSL) on sediments,
44 electron spin resonance (ESR) on fluvial sediments and coupled ESR and U-series on teeth. For open-area localities, at
45 least one of these palaeodosimetric methods can generally be applied but, if several methods are used at the same
46 time and show geochronological discrepancy, the lack of completely independent age control drastically complicates
47 the chronological and archaeological interpretation.

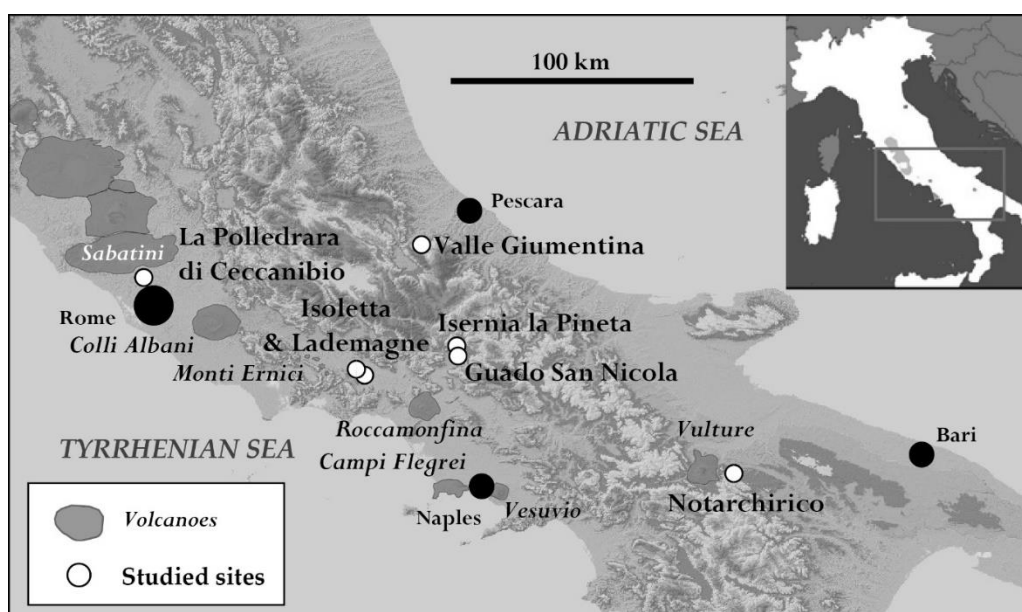
48 However, it is possible in some areas of the European continent to benefit of the combine application of inde-
49 pendent dating methods. It is the case in Central and Southern Italy where the stratigraphic sequences of numerous
50 Palaeolithic sites, very rich in both archaeological and palaeontological remains, contain tephra deposits and record
51 hence the regional volcanic history. The study of such sequences allows hence the comparison of the chronologies
52 derived from ESR and ESR/U-series analyses on fluvial bleached quartz and tooth enamel respectively with the chron-
53 ological framework obtained by $^{40}\text{Ar}/^{39}\text{Ar}$ dating method on single volcanic K-feldspar crystals. The $^{40}\text{Ar}/^{39}\text{Ar}$ method
54 became a reference method for the Quaternary chronology as evidenced by the geochronological framework of hu-
55 man evolution in East Africa that was established thanks to this technic (see for example Brown et al., 2012 or McDou-
56 gall, 2014).

57 In 2009, in collaboration with Italian and French archaeologists and geologists, we initiated an inter-comparison
58 geochronological project aiming to date by different methods Middle Pleistocene sites of Central and Southern Italy,

59 which displayed both volcanic materials and archaeological levels. On each site, teeth and sediments containing vol-
60 canic minerals, both in primary fallout deposits and in reworked sedimentary layers, as well as sediments containing
61 quartz when present, were systematically sampled. The main results obtained in this inter-comparison project are
62 displayed in this paper and compared to the data derived from paleo-environmental and geological studies in order
63 to improve the chronology of the sites dated by only one method or/and only from the available paleo-environmental
64 data. The present paper synthesizes hence for the first time the data obtained during the project by ESR/U-series and
65 ESR on these Italian sites and compares them with the $^{40}\text{Ar}/^{39}\text{Ar}$ chronology established in parallel for each site, allow-
66 ing a general discussion on the potential and limits of ESR/U-series and ESR technics applied to date Middle Pleistocene
67 sites. Even if the main part of the displayed results are already published in different papers, the main issue of the
68 present methodological article is to compare systematically the dating results obtained by ESR/U-series and ESR with
69 those derived from $^{40}\text{Ar}/^{39}\text{Ar}$ analyses, such systematic discussion with comparison having not really realized before.

71 Sites, sampling and $^{40}\text{Ar}/^{39}\text{Ar}$ chronology

72 From the west to the east, the studied sites are La Polledrara di Cecanibbio, Isoletta, Lademagne (Latium), Guado
73 San Nicola, Isernia La Pineta (Molise), Valle Giumentina (Abruzzo) and Notarchirico (Basilicata) (Figure 1). The strati-
74 graphic sequences of these sites, display both archaeological levels with, for some of them, abundant palaeontological
75 fossils, and either primary volcanic deposits such as tephra, or fluvial or fluvio-lacustrine deposits rich in fresh volcanic
76 minerals reworked from such primary volcanic deposits (Figure 2).



77
78 **Figure 1** - Location of the studied Middle Pleistocene sites in Central and Southern Italy.

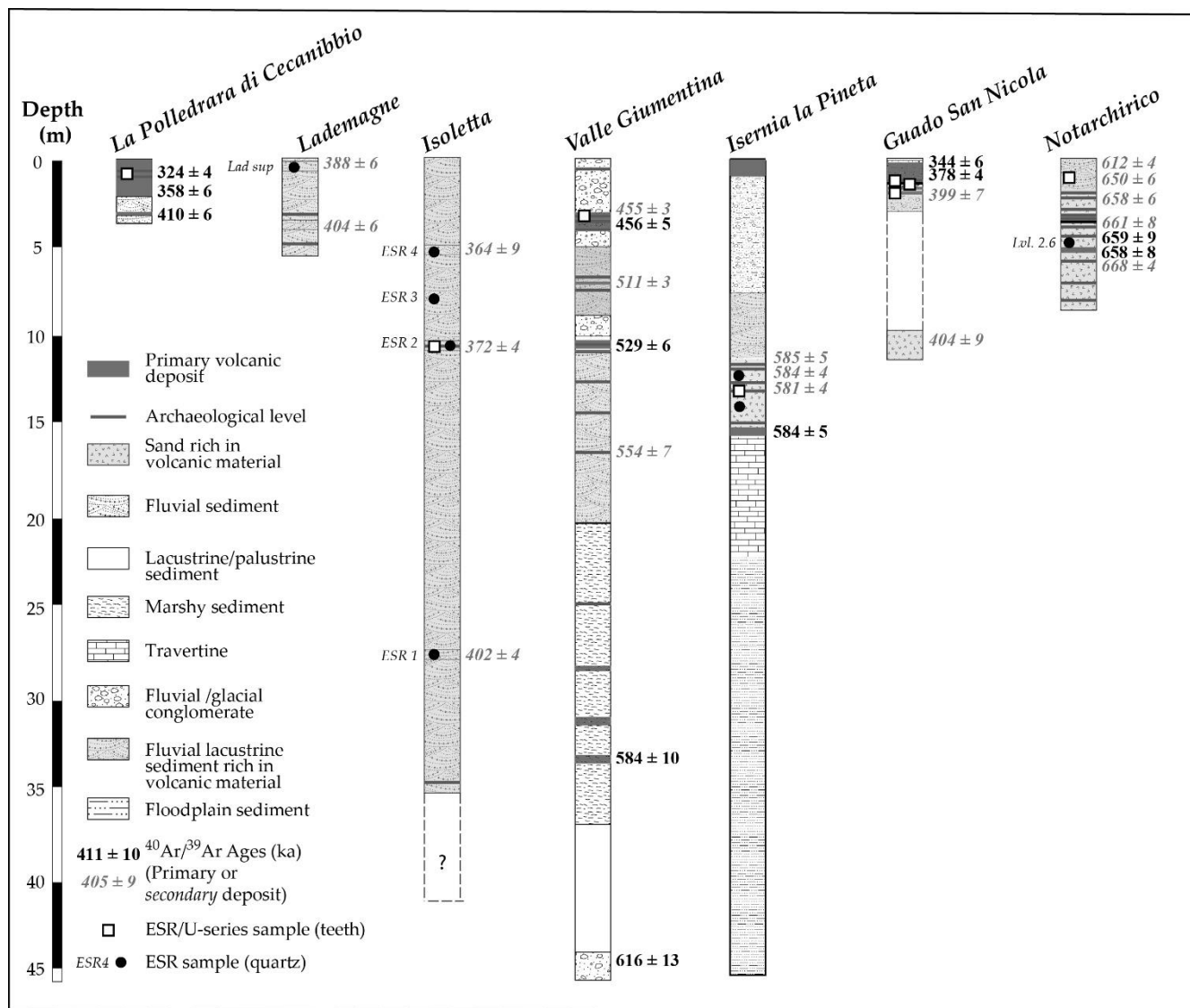


Figure 2 – Simplified stratigraphic logs of the studied Middle Pleistocene sites with indication of the levels dated by ⁴⁰Ar/³⁹Ar and positions of the levels sampled for ESR and ESR/U-series studies. ⁴⁰Ar/³⁹Ar ages were obtained directly on tephra levels (primary deposits) or on potassic feldspar grains extracted from fluvial sediments (secondary deposits), the youngest population corresponding then to a maximum age for the dated level.

La Polledrara di Cecanibbio is located only at 20 km from Rome. Discovered in 1984, the site is since excavated yearly and it is currently considered as one of the richest palaeontological and archaeological deposits of the Latium province, Latium (Anzidei et al., 2004, 2012; Santucci et al., 2016). More than 20 000 palaeontological remains, constituting an assemblage attributed to the Aurelian Large Mammal's stage of the Italian bio-chronological sequence (Palombo and Milli, 2005, Marra et al., 2018; Petronio et al., 2019), and at least 600 artefacts were recovered in fluvial and volcanic lahar sediments rich in pyroclastic minerals originated from the Monti Sabatini volcanic complex. Three different stratigraphic layers and seven *Bos primigenius* teeth were sampled for ⁴⁰Ar/³⁹Ar on single grain and ESR/U-series dating methods respectively (Pereira et al., 2017).

93 Isoletta and Lademagne sites are both located 110 km southeast of Rome in the Frosinone-Ceprano tectonic basin
94 of the Latina Valley, close to the Campogrande locality where was discovered in 1994 the Ceprano human calvarium
95 (Ascenzi et al., 1996; Manzi et al., 2016). Both sequences include mainly fluvial deposits rich in volcanic materials, some
96 tephra layers being deposited also at Isoletta, and several archaeological layers displaying for the upper one Acheulean
97 artefacts (Biddittu, 2004; Biddittu et al., 2012). Several fluvial levels were sampled at Lademagne (n=2) and Isoletta
98 (n=4) for both ESR and $^{40}\text{Ar}/^{39}\text{Ar}$ analyses as well as a cervid tooth from the Acheulean level of Isoletta (Pereira et al.,
99 2018; Voinchet et al., 2020).

100 Isernia La Pineta, 180 km southeast of Rome, is one of the most famous and ancient palaeolithic sites of Italy. It
101 was extensively excavated since its discovery in 1978 and has delivered abundant lithic and faunal remains character-
102 istic of the Middle Galerian Large Mammal's stage. The site was found in a complex stratigraphic sequence including
103 lacustrine, volcanic, fluvial and slope deposits (Coltorti et al., 1982; Peretto et al., 1983, 2015a). A volcanic unit at the
104 base of the archaeological sequence and four teeth (bison and rhinoceros) from the main archaeological unit t3c were
105 sampled as well as sediments (n=2) from the archaeological sequence (Shao et al., 2011; Peretto et al., 2015).

106 The Guado San Nicola site, only 10 km south of Isernia, was discovered in 2005. It site was excavated between
107 2008 and 2012 allowing the recovering of more than 4000 lithic artefacts and 1500 faunal remains. The palaeontolog-
108 ical assemblage is characteristic of the final Italian Galerian stage while the lithic industry includes both Mode 2 and
109 Mode 3 artefacts (Peretto et al., 2016). The archaeological layers are included into a fluvial sequence covered by sev-
110 eral volcanic units attributed to the Roccamonfina volcanic complex (Peretto et al., 2014, 2016). Three different layers
111 of the stratigraphic sequence (tephra and fluvial deposits) and six teeth (horses and rhinoceros) were sampled for
112 $^{40}\text{Ar}/^{39}\text{Ar}$ and ESR/U-series (6 teeth in total) dating methods respectively (Peretto et al., 2016; Pereira et al., 2016).

113 Valle Giumentina is located about 120 km east of Rome and displays a 70m thick sedimentary sequence, mainly
114 constituted by lake shore deposits, in which were found several Palaeolithic levels attributed to the Clactonian and
115 Acheulean in the lower part of the sequence and Levalloisian cultures in the uppermost part respectively (Demangeot
116 and Radmilli, 1953; Nicoud et al., 2015). Numerous tephra layers were also recognized in the stratigraphic (Nicoud et
117 al., 2015; Villa et al., 2016; Degeai et al., 2018). Seven of these volcanic primary deposits sampled all along the se-
118 quence and one cervid tooth extracted from a mandible carried out from an Acheulean level (ALB-42) were dated
119 (Nicoud et al., 2015; Villa et al., 2016; Degeai et al., 2018).

120 Lastly, the early Middle Pleistocene site of Notarchirico is one of the most famous archaeological localities of
121 Southern Italy (Piperno, 1997; Lefèvre et al., 2010). Located 180 km east of Naples close to Monte Vulture stratovol-
122 cano, the site is constituted by a 7m-thick fluvial sequence including eleven archaeological layers. Some of these ar-
123 chaeo-surfaces have delivered handaxes considered as the oldest evidence of Acheulean settlement presently known
124 in Italy (Pereira et al., 2015) and one human femur attributed to *Homo heidelbergensis* (Mallegni et al., 1991). A tephra
125 layer in the lower part of the sequence and several fluvial sediments reworking volcanic minerals were sampled for
126 $^{40}\text{Ar}/^{39}\text{Ar}$, as well as three quartz-rich levels (unit 2.6) and four teeth from the upper palaeo-anthropological layer
127 (supra- α) for ESR and ESR-U-series methods respectively (Voinchet et al., 2020).

128 Details on the analytical $^{40}\text{Ar}/^{39}\text{Ar}$ protocol applied on single volcanic K-feldspar crystals and the main part of the
129 results have been already published in detail (Pereira et al., 2015, 2016, 2017, 2018; Peretto et al., 2015, Villa et al.,
130 2016). These data have permitted to greatly refine the chronology of the studied stratigraphic sequences and associ-
131 ated archaeological levels of the sites.

132 In the present paper, $^{40}\text{Ar}/^{39}\text{Ar}$ ages are presented as weighted mean ages with related full external error at 2σ
133 (analytical + decay constant uncertainties) and as plotted from an inverse isochron diagram ($^{36}\text{Ar}/^{40}\text{Ar}$ vs $^{39}\text{Ar}/^{40}\text{Ar}$).
134 Such diagram permits to assess the isotopic composition of ^{40}Ar trapped at the time of crystallization of the dated
135 minerals and hence evaluate the possibility of argon excess by verifying the assumption that trapped argon isotopes
136 at the eruption time presented the composition of modern atmosphere ($^{40}\text{Ar}/^{36}\text{Ar}$ ratio of 298.56 (Lee et al., 2006)).
137 Ages were re-calculated in the present contribution according the monitor flux standard ACs-2 at 1.1891 Ma (Niespolo
138 e al., 2017) and the K total decay constant of Renne et al. (2011). If the dated samples do not show evidence of such
139 contamination, the calculated inverse isochron age should be equivalent to the weighted mean average one. Inverse
140 isochron $^{40}\text{Ar}/^{36}\text{Ar}$ initial ratio as well as the related calculated ages at 2σ of uncertainties will be therefore displayed.

142 **ESR and ESR/U-series geochronological studies**

143 ESR dating on optically bleached quartz

144 In the case of ESR dating of fluvial quartz grains, the dated event corresponds to the sediment deposition by the
145 river after the exposure of the quartz grains to the sunlight during the river transport phase prior to this deposition.
146 This exposure leads to an optical bleaching of the quartz ESR signals.

147 In the present work, both aluminium (Al) and titanium (Ti) impurity centers are used for dating purpose. It is im-
148 portant to keep in mind that the different Ti signals associated to lithium (Ti-Li) and hydrogen (Ti-H) atoms occurrence

149 in the vicinity of titanium ones can be quickly and completely reset by light exposure which is not the case of Al-signals,
150 probably because of the presence in quartz aluminium centers of “Deep Aluminium Traps” (DAT) that cannot be emp-
151 tied by the energy provided by sunlight (Tissoux et al 2013). It is therefore necessary to determine for each sample the
152 level of "residual" ESR signal intensity, corresponding to the maximum bleaching of the Al-centers into the quartz
153 grains, by exposure of the quartz grains to artificial solar light in the simulator for ca 1600 hours. The “unbleachable”
154 ESR intensity hence obtained subtracted from the ESR signal intensities of the other aliquots of the same sample (in-
155 cluding natural one) before the construction of the growth curve prior to any age calculation.

156 An multi-center ESR approach, based on the systematic measurements of both aluminium (Al), titanium-lithium
157 (Ti-Li) and titanium-hydrogen (Ti-H) signals (Toyoda et al., 2000), was therefore used to date the quartz samples. This
158 method relies on the differences of sensibility of these ESR centers to light. While Ti centers are totally zeroed by
159 sunlight exposure within few hours (Ti-H) or days (Ti-Li), Al-center cannot be completely reset even after several
160 months of exposure. In these conditions, the results obtained for a same sample from these three ESR signals permit
161 to discuss of the quality of the initial bleaching of the quartz grains before deposition on the site or to indicate con-
162 taminations by unbleached quartz grains from older levels or bedrock (Duval and Guilarte, 2015 ; Voinchet et al., 2020).

163 Preparation and measurement protocols used during the present work have been recently displayed by Voinchet
164 et al. (2020). Several sampled sediments did not contain enough quartz to allow an analysis and only 6 quartz samples
165 have been finally analysed: 4 from Isoletta, 1 from Lademagne and 1 from Notarchirico. The equivalent doses and
166 derived ages were calculated from Al- and Ti-centers for all the samples except Notarchirico sample, which not dis-
167 played any Ti-signals, and Lademagne one, for which it was not possible to measure Ti-H signal, undistinguishable to
168 the ESR background noise. For the other samples, the multi-center approach was therefore used. When D_E values
169 obtained from the different centers of a sample were close, a weighted average age was calculated using IsoPlot 3.0
170 (Ludwig, 2003) with 95 % of confidence.

172 ESR/U-series on teeth

173 In the present work, the analysed teeth corresponds to herbivorous cheek teeth (molars or premolars), mainly
174 from bovids but also from equids, rhinoceros and cervids (Table 1).

Site	Sample	Sample laboratory number	Type of analysed tooth
La Polledrara di Cecanibbio	Po2012-01	IPH-2012-51	Cheek tooth Bovidae
	Po2012-02	IPH-2012-52	Cheek tooth Bovidae
	Po2012-03	IPH-2012-53	Cheek tooth Bovidae

	Po2012-04	IPH-2012-54	Cheek tooth Bovidae
	Po2012-05	IPH-2012-55	Cheek tooth Bovidae
	Po2012-06	IPH-2012-56	Cheek tooth Bovidae
	Po2012-07	IPH-2012-57	Cheek tooth Bovidae
Guado San Nicola	SN1001	IPH-2010-14	Cheek tooth Bovidae
	SN1002	IPH-2010-15	Cheek tooth Bovidae
	SN0902	IPH-2009-27	Cheek tooth Equidae
	SN0906	IPH-2009-31	Cheek tooth Bovidae
	SN1003	IPH-2010-16	Cheek tooth Rhinocerotidae
	SN1004	IPH-2010-17	Cheek tooth Rhinocerotidae
Isoletta	ISOL1401	IPH-2014-28	Cheek tooth Cervidae
Valle Giumentina	VG1501	IPH-2015-04	Cheek tooth Cervidae
Isernia la Pineta	IS0901	IPH-2009-01	Cheek tooth Bovidae
	IS0902	IPH-2009-02	Cheek tooth Bovidae
	IS0903	IPH-2009-03	Cheek tooth Bovidae
	IS0904	IPH-2009-04	Cheek tooth Bovidae
Venosa Notarchirico	VN1201	IPH-2012-38	Cheek tooth Rhinocerotidae
	VN1202	IPH-2012-39	Cheek tooth Rhinocerotidae
	VN1203	IPH-2012-40	Cheek tooth Bovidae
	VN1204	IPH-2012-41	Cheek tooth Bovidae

Table 1 – List and nature of the analysed teeth from several Middle Pleistocene Italian sites

Post-mortem uranium-uptake into the dental tissues leads to the variation of the dose rate over time. This phenomenon, which depends on the nature of the site and the age of the sample, makes the determination of the ESR ages, strongly linked to uranium content, particularly delicate and it is necessary to use mathematical models to describe the evolution of this parameter over time. In order to calculate the age of a given sample, the various data acquired through ESR and U-series analyses are then used to model post-mortem U-uptake in the different tissues followed in some cases by a loss of uranium (leaching) in order to provide an unique age. One of the main interests of this approach is to allow the determination for each dental tissue of a U-uptake parameter calculated from the whole set of analytical data and hence the description of the uranium-uptake kinetics into the considered tissue.

The mathematical algorithm for calculating combined ESR/U-series ages has been recently described by Shao et al. (2014). From the U-series isotopic data (U contents, isotopic ratios $^{234}\text{U}/^{238}\text{U}$, $^{230}\text{Th}/^{234}\text{U}$, $^{222}\text{Rn}/^{230}\text{Th}$), a relationship between the incorporation parameter and time is first determined for each dental tissue. It then becomes possible to simulate the evolution over time of the contributions of the different dental tissues to the dose rate. By adding the simulation of the environmental external dose, it becomes possible to simulate the evolution of the total dose rate over time and then to calculate an age by comparing the D_E value obtained experimentally by ESR with this simulation. From this age, a single value corresponding to the incorporation parameter can be calculated for each tissue. In the case of a simple U-uptake, the age is determined with the *Uranium-series (US) model* (Grün et al., 1988), while in the

193 case of a subsequent slight leaching, the U-uptake can be described with the *accelerating uptake (AU) model* (Shao et
194 al., 2012).

195 It should also be underlined that the main part of the results discussed in the present paper have been soon pub-
196 lished in previous papers (La Polledrara di Cecanibbio, Pereira et al., 2017; Guado San Nicola, Bahain et al., 2014,
197 Pereira et al., 2016; Isernia la Pineta, Shao et al., 2011 ; Isoletta, Pereira et al., 2018) and only results of Venosa No-
198 tarchirico (4 samples) and Valle Giumentina (one sample) are completely unpublished data.

200 *Isochron ESR/U-series dating of teeth*

201 The use of isochrons in teeth ESR dating was proposed in 1993 by Bonnie A. Blackwell and Henry P. Schwarcz to
202 take into account a possible variation of the external dose over time in the age calculation using fixed of U-uptake
203 models (Blackwell and Schwarcz, 1993). If it is assumed that the external dose has not varied over time, a diagram can
204 be drawn showing the equivalent doses determined for several sub-samples of the same tooth as a function of the
205 annual internal dose determined for the same sub-samples using the considered U-uptake model (*isochron*). If the
206 points of this isochron are linearly correlated, then the slope of the regression gives the age of the tooth and its inter-
207 cept with the y-axis gives the accumulated external dose common to all sub-samples. The procedure can then be
208 repeated for other external dose values until the best possible correlation between the data is obtained for a given
209 incorporation pattern. It then becomes possible to discuss the appropriateness of using one intake pattern relative to
210 another for the samples under consideration (Blackwell and Schwarcz, 1993; Blackwell et al., 2001). Very cumbersome
211 to implement and very time-consuming, this approach has unfortunately been little used thereafter.

212 More recently, a slightly modified isochronous approach was used to judge the relevance of the dosimetric recon-
213 struction carried out on samples from the Middle Paleolithic site of Biache-Saint-Vaast, France (Bahain et al., 2015). In
214 this study, several teeth of the same level excavated in the 1980s were dated by ESR/U-series, using for the external
215 dose an *in situ* value measured during the excavation as the site is no longer accessible today. Two age groups were
216 then individualized for the analysed teeth, although the archaeological level is very homogeneous from a paleonto-
217 logical point of view and a mixture of two stocks of different ages seems unlikely.

218 A diagram showing the equivalent dose values as a function of the total internal dose modelled by ESR/U-Th for
219 samples assumed to be of the same age (*isochron plot*) was therefore produced. As the data were highly linearly cor-
220 related, it was possible to confirm on the one hand the relevance of using the *in situ* external dose measured during
221 the excavation and on the other hand to estimate the age of the level under consideration using the equation of the

222 regression line obtained. The intercept of this line with the Y-axis then corresponds to the proportion of the equivalent
 223 dose linked to the external dose. By dividing this value by the annual external dose determined today for the level
 224 under consideration, it is possible to estimate the isochron age of the latter and to compare it with the other available
 225 geochronological data.

226 Isochron estimates was also applied successfully on La Polledrara samples (Pereira et al., 2017), leading to a more
 227 systematic use on other Italian Middle Pleistocene sites when the number of analysed samples allow such use. In the
 228 present work isochron age estimates were therefore determined from Guado San Nicola, Isernia and Notarchirico
 229 samples.

231 Results

232 Results are displayed by methods in Tables 2 ($^{40}\text{Ar}/^{39}\text{Ar}$), 3 (ESR), 4 and 5 (ESR/U-series) but will be discussed site
 233 by site from the youngest one (La Polledrara) to the oldest one (Notarchirico). The $^{40}\text{Ar}/^{39}\text{Ar}$ results permit to constrain
 234 the ages of the dated archaeological sequences and therefore the ages of associated ESR/U-series and ESR samples.

235 Concerning the ESR dating of quartz grains (Table 3), except for Isoletta ESR 1 sample for which the age is drastically
 236 overestimated for both Al and Ti centers, the age estimates derived from both signals for the other samples are globally
 237 in agreement with each other and with the $^{40}\text{Ar}/^{39}\text{Ar}$ ages obtained for the corresponding levels (Voinchet et al., 2020).
 238 While the number of samples is too small to allow a definitive conclusion on this point, these results suggest that the
 239 ESR multi-center protocol used here permit to obtain reliable chronology for Middle Pleistocene fluvial sediments. The
 240 dose rate was calculated from the radionuclides activities derived both from *in situ* gamma-ray spectrometry meas-
 241 urements using NaI detector and laboratory high resolution and low background gamma spectrometer using a hyper-
 242 pure Ge crystal.

Site	Sample	Stratigraphical location of analysed samples	$^{40}\text{Ar}/^{39}\text{Ar}$ ages (ka)	Mean Square Weighted Deviation	Probability fit	Isochron ages (ka)	$^{40}\text{Ar}/^{36}\text{Ar}$ initial ratio
La Polledrara di Cecanibbio (Pereira et al., 2017)	POL 1203 &1201	Pumices inside the archaeological level	324 ± 4	0.7	0.9	323 ± 7	296 ± 3
	POL1202	Pumices from fluvial deposit just below archaeological level	358 ± 6	0.8	0.5	368 ± 18	249 ± 80
	POL1301	Tephra 1m below archaeological level	410 ± 6	0.3	1.0	410 ± 6	295 ± 9
Guado San Nicola (Pereira et al., 2016)	S.U. tufi	Volcanic level at the top of the sequence	344 ± 6	0.2	0.6	339 ± 15	299 ± 8
	S.U. A	Volcanic level just capping the archaeological sequence	378 ± 4	1.0	0.4	376 ± 5	307 ± 11
	S.U. C	Fluvial deposits inside the Lower archaeological level	399 ± 7	0.5	0.9	400 ± 6	292 ± 15

	Volcanic sands	Fluvial deposits 10m below the archaeological sequence	404 ± 9	1.3	0.2	405 ± 10	282 ± 11
Isoletta (Pereira et al., 2018)	ESR 4	Fluvial deposits 5m above the Acheulean archaeological level	364 ± 9	0.3	0.8	/	/
	GA6Z	Sediments of the Acheulean archaeological level	374 ± 4	1.4	0.2	374 ± 4	298 ± 2
	ESR 1	Fluvial sands at the bottom of the studied sequence	402 ± 4	0.9	0.6	400 ± 10	300 ± 4
Lademagne (Pereira et al., 2018)	LAD sup	Sediments at the top of the archaeological sequence	388 ± 6	1.6	0.1	390 ± 7	289 ± 11
	LAD inf	Sediments from a layer located between two archaeological levels	404 ± 6	1.1	0.4	405 ± 7	293 ± 6
Valle Giumentina (Nicoud et al., 2015; Villa et al., 2016; Degeai et al., 2018)	T103b	Sediments of the archaeological level LABM	455 ± 3	0.7	0.7	454 ± 3	297 ± 3
	T109b	Sediments of the archaeological level LAN2	529 ± 6	1.3	0.3	528 ± 6	300 ± 3
	T115	Sediments of the archaeological level LN	554 ± 7	0.6	0.8	554 ± 6	294 ± 1.4
	T32	Tephra below the archaeological sequence	584 ± 10	0.4	0.9	581 ± 17	305 ± 30
	T45	Tephra at the bottom of the sedimentary sequence	616 ± 13	0.2	1.0	617 ± 14	298 ± 4
Isernia la Pineta (Peretto et al., 2015)	3s6-9	Sediments sampled above the main archaeological level t3a	585 ± 5	1.0	0.5	585 ± 5	291 ± 7
	3s10	Sediments sampled above the main archaeological level t3a	581 ± 7	1.4	0.2	581 ± 8	296 ± 4
	3coll	Sediments capping the main archaeological level t3a	581 ± 4	1.2	0.3	583 ± 5	290 ± 10
	U4T	Tephra just below the archaeological sequence	584 ± 5	0.5	1.0	583 ± 7	305 ± 30
Venosa Notarchirico (Pereira et al., 2015; Voinchet et al., 2020)	NOT1.6	Top of the archaeological sequence	612 ± 4	1.5	0.2	612 ± 4	296 ± 2
	NOT 1.5	Sediments capping supra α level	650 ± 6	0.6	1.1	651 ± 6	295 ± 3
	NOT 1.3	Just below supra α level	658 ± 6	0.1	1.2	657 ± 11	298 ± 36
	NOT 2.6	Just below D level	661 ± 8	0.7	0.6	658 ± 9	294 ± 9
	NOT 2.2	Tephra between level E and F	659 ± 9	0.3	1.0	663 ± 10	291 ± 6
	NOT 2.1	Tephra between level E and F	658 ± 8	0.6	0.6	657 ± 8	304 ± 14
	U.3	Sediments just below F level	668 ± 4	1.8	0.1	668 ± 4	297 ± 4

244

245

Table 2 – $^{40}\text{Ar}/^{39}\text{Ar}$ ages obtained from volcanic minerals recovered from several Middle Pleistocene Italian sites.

246

The indicated $^{40}\text{Ar}/^{39}\text{Ar}$ age corresponds to the age of the youngest homogeneous potassic feldspars population. These ages

247

were re-calculated in the present contribution according to the monitor flux standard ACs-2 at 1.1891 Ma (Niespolo et al., 2017)

248

and the K total decay constant of Renne et al. (2011) from the original data published in the various referred papers. A homogeneous population is considered relevant when the weighted mean of these crystals has the following statistical characteristics:

249

MSWD < 1.5, Probability fit \geq 0.1. The weighted average ages were calculated using IsoPlot 3.0 (Ludwig, 2003) and given at 95%

250

(2 σ) of confidence.

251

252

Site	Sample	ESR signal	D $_{\alpha}$ ($\mu\text{Gy/a}$)	D $_{\beta}$ ($\mu\text{Gy/a}$)	D $_{\gamma}$ ($\mu\text{Gy/a}$)	D $_{\text{cosmic}}$ ($\mu\text{Gy/a}$)	W (%)	δ_{bl} (%)	D $_{\text{a}}$ ($\mu\text{Gy/a}$)	D $_{\text{E}}$ (Gy)	Age (ka)	Mean Age (ka)	$^{40}\text{Ar}/^{39}\text{Ar}$ Age (ka)
Isoletta (Pereira et al., 2018 ; Voinchet et al., 2020)	Isoletta ESR 1	Ti-H	19±1	190±11	168±10	24±1	15	100	401±15	325 ± 29	810 ± 47	-	402 ± 4
		Ti-Li	19±1	190±11	168±10	24±1	15	100	401±15	715±75	1786 ± 327		
		Al	19±1	190±11	168±10	24±1	15	48	401±15	462±24	1154 ± 109		
	Isoletta ESR 2	Ti-H	57±2	1786±36	1008±28	33±2	14	100	2884±15	295 ± 20	102 ± 16	442±58	374 ± 4
		Ti-Li	57±2	1786±36	1008±28	33±2	14	100	2884±15	1155±110	401 ± 59		
		Al	57±2	1786±36	1008±28	33±2	14	42	2884±15	1315±62	456 ± 34		
	Isoletta ESR 3	Ti-H	30±2	497±20	354±16	53±3	12	100	934±26	349±24	374±17	349±26	364 ± 9 < X < 374 ± 4
		Ti-Li	30±2	497±20	354±16	53±3	12	100	934±26	314±73	336 ± 66		
		Al	30±2	497±20	354±16	53±3	12	46	934±26	338±60	362 ± 64		
	Isoletta	Ti-H	20±1	303±12	220±10	101±5	15	100	644±16	243±15	374±84	396±83	364 ± 9

	ESR 4	Ti-Li	20±1	303±12	220±10	101±5	15	100	644±16	275±25	426 ± 59			
		Al	20±1	303±12	220±10	101±5	15	45	644±16	252±40	391 ± 72			
Lademagne (Pereira et al., 2018 ; Voinchet et al., 2020)	Lademagne Sup	Ti-H	Unmeasurable										402±71	388 ± 6
		Ti-Li	77±3	980±35	919±52	111±6	5	100	2088±70	831±70	398 ± 51			
		Al	77±3	980±35	919±52	111±6	5	44	2088±70	847±100	406 ± 51			
Venosa Notarchirico (Pereira et al., 2015; Voinchet et al., 2020)	Level 2-6	Ti-H	Unmeasurable										-	612 ± 4 < X < 661 ± 8
		Ti-Li	Unmeasurable											
		Al	84±1	1999±24	1803±21	166±8	10	57	4052±32	2660±122	657 ± 31			

Table 3 – ESR data and ages for sediments recovered from several Middle Pleistocene Italian sites.

Equivalent doses (D_E) were derived from the obtained intensity growth curves using an exponential + linear function for Al and Ti-Li centers (Duval et al., 2009; Voinchet et al., 2013) and by a single saturating exponential function for Ti-H from the six first points of the growth curves (Voinchet et al., 2020) with Microcal OriginPro 8 software, both with $1/I^2$ weighting (according with Yokoyama et al., 1985). Age calculations were performed using the following parameters: dose-rate conversions factors from Guérin et al. (2011); a k-value of 0.15 ± 0.1 (Laurent et al., 1998); alpha and beta attenuations from Brennan (2003) and Brennan et al. (1991); water attenuation formulae from Grün (1994); cosmic dose rate estimated from the Prescott and Hutton's equations (1994). The internal dose rate was considered as negligible because of the low contents of radionuclides usually found in quartz grains (Murray and Roberts 1997; Vandenbergue et al. 2008). ESR age estimates are given with one sigma error range.

Concerning the ESR/U-series results (Tables 4 and 5), when several teeth from a same archaeological level were analysed, the obtained age estimates are displayed both by age density probability plots and isochron plots (Figure 3) and are compared with the available $^{40}\text{Ar}/^{39}\text{Ar}$ and ESR dates (Figure 4). The age density plots build from the ESR/U-series age estimated with IsoPlot 3.0 software (Ludwig, 2003) permit to observe the homogeneity of the obtained age results and to determine mean ages for each eventual age populations. In complement, the isochron approach (Blackwell and Schwarcz, 1993) allows the evaluation of the quality of the dose rate reconstruction by comparison of the respective weight of accumulated external and internal dose contributions, the last one evolving with time according with the U-uptake modelling in each dental tissue. It permits to estimate an age estimate for a given level by plotting the accumulated internal doses modelled for the teeth vs the D_E and by dividing the intercept value ($x=0$, that represents the corresponding accumulated external doses) by the "real" external dose rates used for the age calculation. These two graphic representations permit to better discuss of the results.

Site	Samples	Tissue	U content (ppm)	$^{234}\text{U}/^{238}\text{U}$	$^{230}\text{Th}/^{232}\text{Th}$	$^{230}\text{Th}/^{234}\text{U}$	Apparent U-series age (ka)	$^{222}\text{Rn}/^{230}\text{T}$ h	Initial thickness (μm)	Removed thickness Internal side (μm)	Removed thickness External side (μm)
La Polledrara di Cecanibio (Pereira et al., 2017)	Po2012-01	dentine	342.83 \pm 9.12	1.215 \pm 0.008	20	0.658 \pm 0.030	112 \pm 9	0.351	1270 \pm 159	172 \pm 21	32 \pm 4
		enamel	9.89 \pm 0.26	1.131 \pm 0.021	> 100	0.760 \pm 0.034	149+16/-13	0.612			
	Po2012-02	dentine	294.18 \pm 9.96	1.172 \pm 0.033	48	0.617 \pm 0.027	101 +8/-7	0.395	1323 \pm 165	116 \pm 14	6 \pm 1
		enamel	10.11 \pm 0.33	1.148 \pm 0.039	13	0.798 \pm 0.039	164+23/-18	1.000			
	Po2012-03	dentine	283.76 \pm 8.81	1.215 \pm 0.031	> 50	0.575 \pm 0.025	90+7/-6	0.390	1124 \pm 140	191 \pm 24	86 \pm 11
		enamel	23.52 \pm 0.83	1.153 \pm 0.044	46	0.629 \pm 0.032	105+10/-9	0.321			
	Po2012-04	dentine	326.73 \pm 8.79	1.209 \pm 0.026	> 100	0.646 \pm 0.026	108+8/-7	0.426	1394 \pm 174	43 \pm 5	114 \pm 14
		enamel	13.80 \pm 0.49	1.387 \pm 0.053	> 50	0.704 \pm 0.034	122+12/-11	0.497			
	Po2012-05	dentine	273.00 \pm 9.22	1.239 \pm 0.036	> 50	0.633 \pm 0.033	105+10/-9	0.533	1238 \pm 155	109 \pm 14	78 \pm 10
		enamel	9.98 \pm 0.28	1.185 \pm 0.023	> 50	0.699 \pm 0.033	125+12/-11	0.557			
	Po2012-06	dentine	340.53 \pm 11.61	1.252 \pm 0.034	> 100	0.503 \pm 0.027	74 \pm 6	0.385	1339 \pm 167	225 \pm 28	155 \pm 19
		enamel	8.92 \pm 0.25	1.164 \pm 0.024	> 100	0.679 \pm 0.037	119+13/-12	0.650			
	Po2012-07	dentine	396.22 \pm 13.70	1.062 \pm 0.030	> 100	0.654 \pm 0.035	114+12/-11	0.279	1376 \pm 172	138 \pm 17	75 \pm 9
		enamel	5.72 \pm 0.24	1.473 \pm 0.061	> 100	0.724 \pm 0.035	127+13/-11	0.780			
Guado San Nicola (Bahain et al., 2014; Pereira et al., 2016)	SN1001	cement	40.76 \pm 0.09	1.319 \pm 0.004	> 100	1.133 \pm 0.008	> 500	0.290	1053 \pm 132	68 \pm 8	12 \pm 1
		dentine	103.67 \pm 0.45	1.253 \pm 0.003	> 100	0.950 \pm 0.011	251 \pm 12	0.407			
		enamel	2.45 \pm 0.01	1.303 \pm 0.004	42	0.897 \pm 0.011	207 \pm 8	0.796			
	SN1002	cement	108.95 \pm 0.44	1.234 \pm 0.004	> 100	0.840 \pm 0.007	180 \pm 5	0.352	1204 \pm 151	67 \pm 8	13 \pm 2
		dentine	121.74 \pm 0.45	1.248 \pm 0.004	> 100	0.831 \pm 0.009	175 \pm 6	0.352			
		enamel	2.96 \pm 0.01	1.281 \pm 0.004	> 50	0.765 \pm 0.008	145 \pm 4	0.705			
	SN0902	cement	38.99 \pm 0.11	1.319 \pm 0.003	> 50	1.167 \pm 0.007	> 500	0.307	1273 \pm 159	32 \pm 4	80 \pm 10
		dentine	140.33 \pm 0.43	1.204 \pm 0.003	> 100	0.855 \pm 0.005	190 \pm 4	0.419			
	SN0906	dentine	67.27 \pm 0.27	1.338 \pm 0.006	> 100	1.048 \pm 0.010	365 \pm 31	0.085	1793 \pm 224	48 \pm 6	58 \pm 7
		enamel	1.35 \pm 0.01	1.254 \pm 0.006	7	1.114 \pm 0.010	> 500	0.779			
	SN1003	dentine	86.26 \pm 0.21	1.328 \pm 0.004	> 100	1.055 \pm 0.009	384 \pm 31	0.363	2328 \pm 291	56 \pm 7	28 \pm 4
		enamel	0.50 \pm 0.01	1.230 \pm 0.006	3	0.934 \pm 0.012	241 \pm 14	0.790			
	SN1004	dentine	83.68 \pm 0.38	1.318 \pm 0.003	> 100	1.051 \pm 0.010	379 \pm 29	0.411	1896 \pm 237	67 \pm 8	40 \pm 5
		enamel	0.71 \pm 0.01	1.402 \pm 0.005	16	0.918 \pm 0.011	213 \pm 9	0.644			
Isernia la Pineta (Shao et al., 2011)	IS0901	cement	120.33 \pm 0.77	1.327 \pm 0.009	> 100	0.770 \pm 0.018	146 \pm 9	0.265	1098 \pm 137	68 \pm 9	108 \pm 13
		dentine	225.20 \pm 1.07	1.314 \pm 0.005	> 100	0.720 \pm 0.008	129 \pm 3	0.255			
		enamel	3.78 \pm 0.02	1.355 \pm 0.001	26	0.673 \pm 0.023	114 \pm 9	0.647			
	IS0902	dentine	193.61 \pm 0.95	1.276 \pm 0.005	> 100	0.695 \pm 0.010	122 \pm 4	0.250	1269 \pm 159	153 \pm 19	88 \pm 11
		enamel	3.25 \pm 0.01	1.343 \pm 0.001	12	0.691 \pm 0.031	120 \pm 2	0.479			
	IS0903	cement	216.03 \pm 1.04	1.253 \pm 0.010	> 50	0.621 \pm 0.014	146 \pm 9	0.182	1212 \pm 151	115 \pm 14	53 \pm 7
		dentine	237.29 \pm 1.07	1.263 \pm 0.005	> 100	0.574 \pm 0.009	129 \pm 3	0.238			
		enamel	4.39 \pm 0.01	1.320 \pm 0.001	43	0.543 \pm 0.016	82 \pm 4	0.564			
	IS0904	cement	126.93 \pm 0.97	1.362 \pm 0.013	22	0.901 \pm 0.015	205 \pm 13	0.173	1323 \pm 165	243 \pm 30	101 \pm 13
		dentine	201.84 \pm 1.14	1.276 \pm 0.005	> 100	0.686 \pm 0.009	119 \pm 4	0.239			
		enamel	2.62 \pm 0.01	1.343 \pm 0.001	9	0.683 \pm 0.037	118 \pm 14	0.598			
	Venosa Notarchirico Level supra α (this work)	VN1201	dentine	246.25 \pm 1.77	1.153 \pm 0.009	20	0.892 \pm 0.010	217 \pm 8	0.972	1254 \pm 157	283 \pm 35
enamel			3.19 \pm 0.01	1.153 \pm 0.001	> 50	0.532 \pm 0.002	81 \pm 1	1.000			
VN1202		dentine	216.96 \pm 1.68	1.164 \pm 0.011	36	0.743 \pm 0.012	141 \pm 5	0.842	1469 \pm 184	255 \pm 32	58 \pm 7
		enamel	11.10 \pm 0.04	1.174 \pm 0.006	35	0.638 \pm 0.005	107 \pm 1	1.000			
VN1203		cement	158.83 \pm 1.23	1.246 \pm 0.008	25	1.020 \pm 0.013	342 \pm 26	0.733	1105 \pm 138	92 \pm 12	124 \pm 16
		dentine	197.72 \pm 2.32	1.307 \pm 0.012	39	1.056 \pm 0.017	398 \pm 54	0.638			
VN1204		dentine	140.80 \pm 0.73	1.458 \pm 0.008	> 50	1.078 \pm 0.008	380 \pm 21	0.679	1172 \pm 146	190 \pm 24	163 \pm 20
		enamel	5.77 \pm 0.01	1.306 \pm 0.003	> 50	1.140 \pm 0.004	> 500	0.671			
Isoletta (Pereira et al., 2018)	ISOL1401	dentine	109.86 \pm 9.97	1.281 \pm 0.027	31	0.865 \pm 0.036	190 +23/-19	0.865	1078 \pm 100	98 \pm 12	67 \pm 8
		enamel	1.65 \pm 0.07	1.316 \pm 0.063	> 100	0.953 \pm 0.057	245 +76/-44	0.953			
Valle Giumentina (this work)	VG1501	dentine	53.67 \pm 1.67	1.426 \pm 0.038	> 50	1.078 \pm 0.052	> 300	0.898	1063 \pm 100	118 \pm 15	109 \pm 14
		enamel	1.60 \pm 0.07	1.316 \pm 0.060	4	1.058 \pm 0.061	> 300	0.364			

274 **Table 4** – U-series and ESR data for the analysed teeth recovered from several Middle Pleistocene Italian sites.

275 U-series analyses were performed on each dental tissue in order to determine the U-uptake parameters necessary to the dose
276 rate contributions and age calculations (see details in Shao et al., 2015b), either by alpha spectrometry (MNHN, Paris), or by
277 Neptune Multi-Collector Inductively Coupled Plasma Mass Spectrometer (MC-ICPMS) (Nanjing Normal University, China).

Site	Samples	Tissue	D _E (Gy)	U uptake parameters p (regular) or n (<i>italics</i>)	D _a α internal (μGy/a)	D _a β (μGy/a)	D _a (γ + cosm) (μGy/a)	D _a total (μGy/a)	ESR/U-series (US or AU) ages (ka)	⁴⁰ Ar/ ³⁹ Ar ages, ESR/U-series density plot and ESR/U-series isochron age estimates (ka)
La Polledrara di Cecanibbio (Pereira et al., 2017)	Po2012-01	dentine enamel	1665 ± 169	-0.360 ± 0.151 0.280 ± 0.248	1779 ± 868	708 ± 183	2716 ± 40	5203 ± 888	320 ± 44	⁴⁰ Ar/ ³⁹ Ar age 324 ± 4
	Po2012-02	dentine enamel	1902 ± 105	-0.593 ± 0.027 0.221 ± 0.172	2691 ± 696	1150 ± 212	2716 ± 40	6557 ± 729	290 ± 28	
	Po2012-03	dentine enamel	1845 ± 141	0.208 ± 0.234 0.580 ± 0.287	2361 ± 487	1074 ± 52	2716 ± 40	6151 ± 702	300 ± 29	ESR/U-series density plot ages Two populations 196 ± 25 (n=2) 324 ± 25 (n=4)
	Po2012-04	dentine enamel	1718 ± 48	-0.683 ± 0.112 -0.538 ± 0.135	3008 ± 955	1902 ± 530	2716 ± 40	7626 ± 1093	183 ± 23	
	Po2012-05	dentine enamel	1421 ± 89	-0.076 ± 0.088 0.304 ± 0.114	1472 ± 314	1230 ± 200	2716 ± 40	5418 ± 375	317 ± 20	ESR/U-series isochron age Two populations ≈ 153 (n=2) ≈ 321 (n=4)
	Po2012-06	dentine enamel	1500 ± 104	-0.128 ± 0.137 1.076 ± 0.263	1388 ± 528	863 ± 233	2716 ± 40	4968 ± 578	286 ± 28	
	Po2012-07	dentine enamel	1248 ± 35	-0.641 ± 0.068 -0.489 ± 0.084	1566 ± 338	1928 ± 360	2716 ± 40	6211 ± 495	201 ± 15	
Guado San Nicola (Bahain et al., 2014; Pereira et al., 2016)	SN1001	cement dentine enamel	1029 ± 31	-0.0051 ± 0.0005 -0.0042 ± 0.0005 -0.0038 ± 0.0005	643 ± 154	1211 ± 211	1560 ± 150	3408 ± 301	302 ± 25	⁴⁰ Ar/ ³⁹ Ar ages 378 ± 4 < X < 399 ± 7
	SN1002	cement dentine enamel	1153 ± 20	-0.549 ± 0.106 -0.518 ± 0.111 -0.250 ± 0.150	584 ± 233	1170 ± 329	1560 ± 150	3304 ± 430	349 ± 45	
	SN0902	cement dentine enamel	1193 ± 45	-0.0038 ± 0.0001 -0.0025 ± 0.0001 -0.0015 ± 0.0001	605 ± 160	1072 ± 223	1560 ± 150	3237 ± 313	369 ± 33	ESR/U-series density plot ages Two populations 311 ± 35 (n=3) 364 ± 38 (n=3)
	SN0906	dentine enamel	815 ± 26	-0.0042 ± 0.0001 -0.0044 ± 0.0001	438 ± 122	563 ± 96	1560 ± 150	2554 ± 216	319 ± 25	
	SN1003	dentine enamel	698 ± 74	-0.0037 ± 0.0001 -0.0033 ± 0.0001	128 ± 272	283 ± 126	1560 ± 150	1971 ± 335	354 ± 47	ESR/U-series isochron age Two populations Non calculable (n=3) ≈ 366 (n=3)
	SN1004	enamel	887 ± 45	-0.0035 ± 0.0004 -0.0028 ± 0.0004	204 ± 107	605 ± 172	1560 ± 150	2365 ± 227	373 ± 35	
Isernia la Pineta (Shao et al., 2011)	IS0901	cement dentine enamel	1645 ± 113	0.071 ± 0.167 0.385 ± 0.210 0.743 ± 0.256	448 ± 37	1264 ± 76	1910 ± 50	3622 ± 99	456 ± 54	⁴⁰ Ar/ ³⁹ Ar age X < 584 ± 5
	IS0902	dentine enamel	1238 ± 61	0.323 ± 0.184 0.362 ± 0.187	401 ± 28	713 ± 43	1990 ± 50	3104 ± 71	400 ± 42	
	IS0903	cement dentine enamel	1360 ± 88	1.275 ± 0.343 1.796 ± 0.413 2.200 ± 0.466	284 ± 30	888 ± 66	1720 ± 50	2892 ± 88	471 ± 59	ESR/U-series density plot ages 435 ± 48 (n=3) ESR/U-series isochron age ≈ 585 (n=3)
	IS0904	cement dentine enamel	1455 ± 89	-0.551 ± 0.072 0.563 ± 0.206 0.599 ± 0.209	321 ± 23	1043 ± 42	1945 ± 50	3309 ± 69	441 ± 46	
Venosa Notarchirico (this work)	VN1201	dentine enamel	751 ± 20	-1.000 -0.151 ± 0.282	445 ± 127	2075 ± 546	1092 ± 55	3612	208 ± 32	⁴⁰ Ar/ ³⁹ Ar 612 ± 4 < X < 658 ± 8
	VN1202	dentine enamel	1596 ± 77	0.479 ± 0.217 1.475 ± 0.344	1128 ± 327	701 ± 165	1092 ± 55	2921 ± 370	546 ± 64	
	VN1203	cement dentine enamel	2078 ± 79	-0.0044 ± 0.0006 -0.0045 ± 0.0006 -0.898 ± 0.024	2352 ± 487	3402 ± 502	1092 ± 55	6836 ± 702	304 ± 29	ESR/U-series density plot ages Non calculable ESR/U-series isochron age ≈ 134 (n=3)
	VN1204	dentine enamel	1889 ± 80	-0.0029 ± 0.0003 -0.0032 ± 0.0003	2026 ± 329	1350 ± 200	1092 ± 55	4477 ± 389	422 ± 32	
Isoletta (Pereira et al., 2018)	ISOL1401	dentine enamel	1151 ± 33	-0.578 ± 0.063 -0.0031 ± 0.0004	553 ± 125	1063 ± 194	1494 ± 150	3110 ± 275	370 ± 31	⁴⁰ Ar/ ³⁹ Ar age 374 ± 4
Valle Giumentina (this work)	VG1501	dentine enamel	1577 ± 51	-0.0027 ± 0.0002 -0.0027 ± 0.0002	405 ± 110	800 ± 175	2307 ± 150	3512 ± 254	449 ± 29	⁴⁰ Ar/ ³⁹ Ar age X < 455 ± 3

279 The equivalent doses D_E were extrapolated from the obtained dose-response data sets using either The growth curves were built
280 for each sample using different fitting functions (single saturating exponential, SSE, according with Apers et al., 1981; double sat-
281 urating exponential function (DSE), according with Duval et al. (2009), or exponential plus linear function (E+L), according with
282 Shao et al. (2015a). The equivalent dose corresponding to the function that best describes the experimental data and gives the
283 best statistics is then used to calculate age.

284 The radioelement contents of sediment samples associated to each tooth were determined by in laboratory high resolution low
285 background gamma spectrometry and *in situ* gamma measurements with TL Al_2O_3 dosimeters at La Polledrara and Inspector 1000
286 Canberra gamma spectrometer on the other sites. A sediment water content value of $15 \pm 5\%$ was therefore assumed for the age
287 calculations. The cosmic dose rate was estimated using the formula of Prescott and Hutton (1994). Were also used the following
288 parameters: a k-value (α efficiency) of 0.13 ± 0.02 (Grün and Katzenberger-Apel, 1994); water content of 0 wt% in the enamel and
289 7 wt% in the dentine and cementum; conversion contents-doses factors from Guérin et al.; (2011). For each dental tissue, Rn loss
290 was estimated from both gamma and alpha/ICP measurements (Bahain et al., 1992). The beta dose contributions were corrected
291 from the enamel part destroyed on each side of the enamel layer during the preparation process (according to Brennan et al.,
292 1997).

293 ESR/U-series ages, different dose-rate contributions and U-uptake parameters were then calculated using either US model (Grün
294 et al., 1988) or AU model (Shao et al., 2012). The "USESR", "AUESR" and "combined ESR" computer programs were used for the
295 age calculation in which the age uncertainty (1σ) is calculated with Monte Carlo approach (Shao et al., 2014).

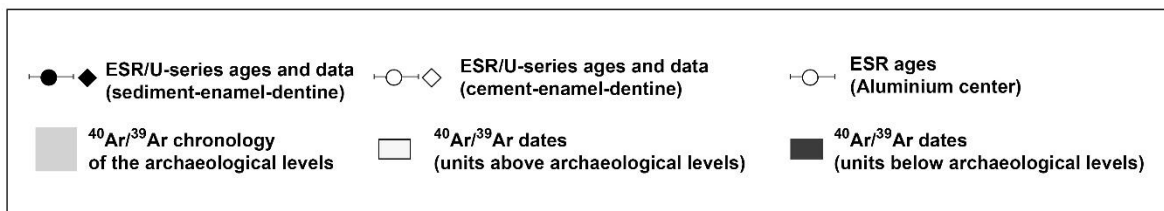
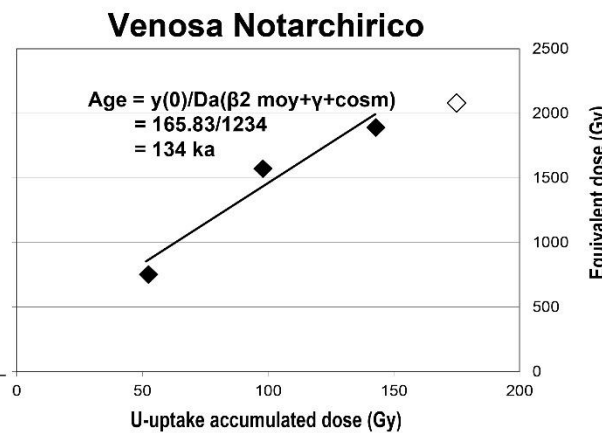
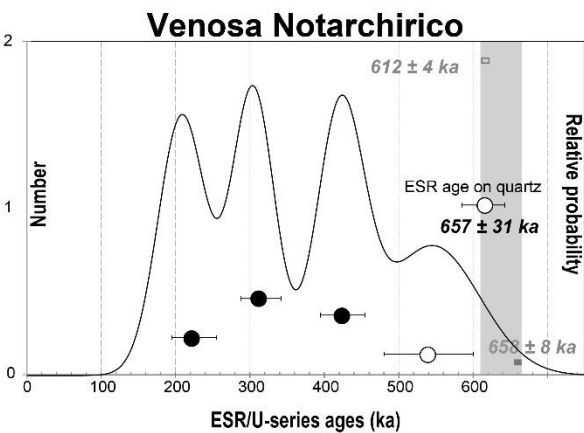
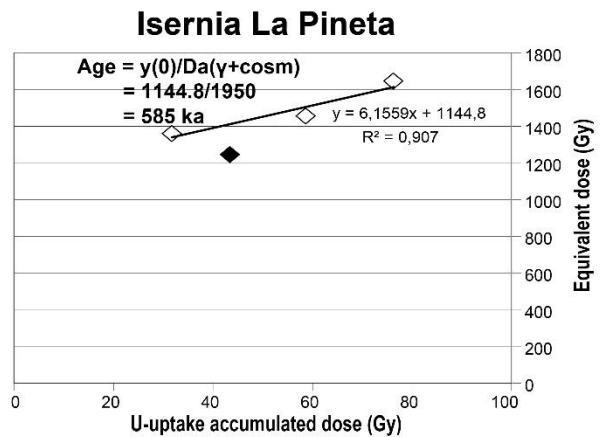
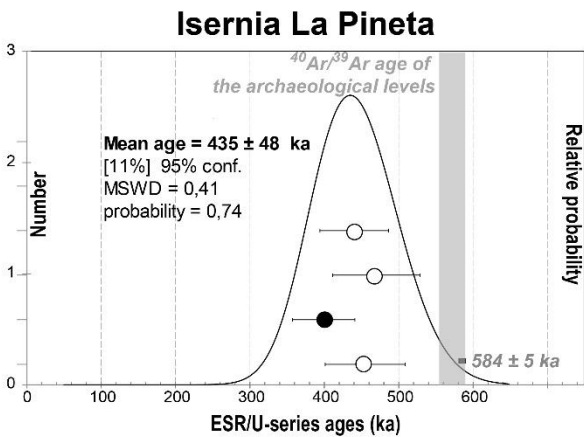
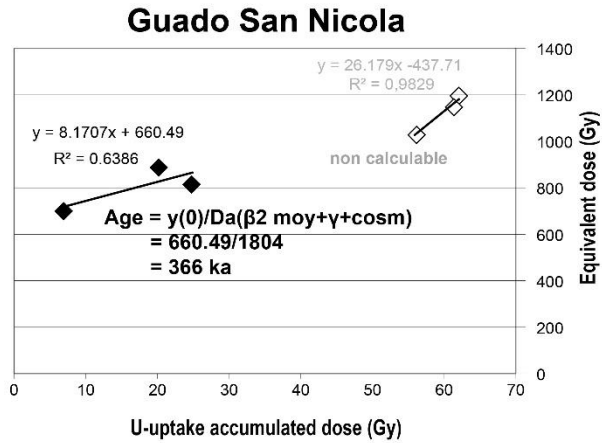
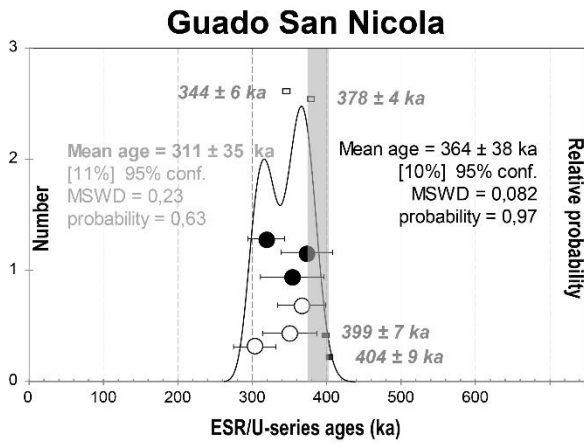
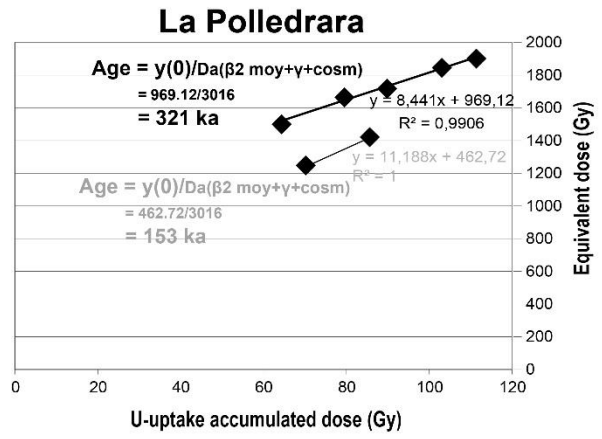
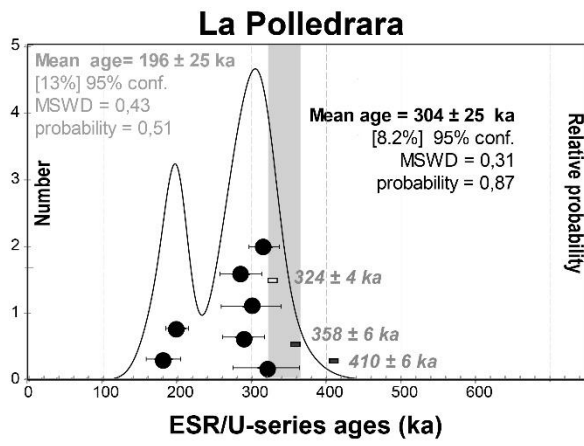
296 Isochron age estimates were newly determined in the present work except for La Polledrara samples (Pereira et al., 2017).

297

298

299

300



302 **Figure 3** – Age density probability plots (left, built using Isoplot 3.0 software, Ludwig, 2003) and isochron plots (right) obtained for
303 the different studied Middle Pleistocene sites of Central and Southern Italy with indication of the corresponding $^{40}\text{Ar}/^{39}\text{Ar}$ chro-
304 nology. The U-uptake accumulated dose corresponds to the sum of the internal (enamel) and beta dose (corresponding to dentine
305 and eventually cement) reconstructed for the considered sample all along its geological history from the modelled uptake param-
306 eters.

308 La Polledrara di Cecanibbio

309 According with the $^{40}\text{Ar}/^{39}\text{Ar}$ dates, the age of the teeth from La Polledrara di Cecanibbio upper archaeological
310 level should be close to 324 ± 4 ka, since the altered pumices extracted from this level are geologically contempora-
311 neous of the animal death and associated archaeological remains. The age density plot obtained using the ESR/U-
312 series results is bimodal and the ages are variably (1-43%) underestimated. It was interpreted in previous paper as
313 reflecting a poor dosimetric reconstruction of the internal dose rate evolution, in relation with the high U-content
314 measured in the different dental tissues of the analysed teeth (Pereira et al., 2017). However, it should be noticed for
315 part of the teeth that the isochron curves provide generally an age close to the $^{40}\text{Ar}/^{39}\text{Ar}$ estimates, especially for teeth
316 without cement, that seems indicate that the measured external doses are well representative to the received histor-
317 ical dose. The isochron age (321 ka) obtained for 5 of the 7 analysed teeth, is similar than the oldest age mode obtained
318 for the teeth of this site and is coherent with the $^{40}\text{Ar}/^{39}\text{Ar}$ age of this specific volcanic event. On the other hand, the
319 isochron plot built from the apparent younger teeth population provide severely underestimated date that could re-
320 flect the record of an event posterior to the archaeological sequence deposition, such as the opening of the present-
321 day landscape, which would lead to a drastic change of the dosimetric environmental conditions for these teeth.

322
323 Isoletta – At Isoletta, three layers were dated by $^{40}\text{Ar}/^{39}\text{Ar}$ (Pereira et al., 2018). The age of the volcanic layer in
324 which ESR 1 quartz sample was collected is 402 ± 4 ka, while the level corresponding to ESR 4 sample, at the top of the
325 sequence, gives an age of 364 ± 9 ka.

326 The ESR results obtained for Isoletta sediments are consistent within 1σ with this $^{40}\text{Ar}/^{39}\text{Ar}$ chronology, except for
327 ESR1 sample for which severe overestimation is observed whatever the center used, due probably to both an incom-
328 plete initial bleaching of these ESR centers and a poor dose rate evaluation (Voinchet et al., 2020). Two samples (ESR4
329 and ESR3) provided similar ages for the three centers while the age obtained using Ti-H center is underestimated for
330 ESR2 sample. Voinchet et al. (2020) suggest that Ti-H center cannot be used to determine reliable D_E estimates higher

331 than 300–400 Gy due to signal saturation, explaining such underestimation. Weighted mean ages of 442 ± 58 ka (ESR2,
332 2σ , Full external error, MSWD = 0.65 and $P = 0.42$), 349 ± 26 ka (ESR 3, 2σ , full external uncertainty, MSD = 2.08 and P
333 = 0.059) and 396 ± 41 ka (ESR 4, 2σ , full external error, MSWD = 0.27 and $P = 0.76$) were obtained for these 3 sediments.
334 The ESR/US age estimate obtained for Isoletta tooth sample, 370 ± 31 ka, agrees with both ESR dates from overlying
335 and underlying sediments and similar to the $^{40}\text{Ar}/^{39}\text{Ar}$ age of this archaeological level, 374 ± 4 ka.

336 Lademagne - At Lademagne, $^{40}\text{Ar}/^{39}\text{Ar}$ chronology places the age of the archaeological levels between 404 ± 6 ka
337 (Lad inf) and 388 ± 6 ka (Lad sup), providing hence a *terminus ante quem* for the level dated by ESR (Pereira et al.,
338 2018). The ESR ages calculated from Ti-Li (398 ± 51 ka) and Al (406 ± 51 ka) signals are consistent, yielding a weighted
339 mean age of 402 ± 71 ka (2σ , Full external error, MSWD = 0.012 and $P = 0.91$).

340 Guado San Nicola - The $^{40}\text{Ar}/^{39}\text{Ar}$ data obtained chronologically place the human occupations between 404 ± 9
341 ka and 378 ± 4 ka (Pereira et al., 2016), a result considered then quite surprising in relation with the occurrence of
342 Mode 3 archaeological artefacts in these levels. Here again, the age density plots built from ESR/U-series results is
343 bimodal and the age underestimation, 1-20% lower than the $^{40}\text{Ar}/^{39}\text{Ar}$ ages, was interpreted in previous paper as re-
344 lated with the high U-content measured in the different dental tissues of the analysed teeth (Pereira et al., 2016). The
345 isochron age derived from the teeth without cement, around 365 ka, is however close from the older ESR/U-series age
346 population, 364 ± 38 ka, and, taking into account uncertainties associated with this result, in agreement with the
347 $^{40}\text{Ar}/^{39}\text{Ar}$ age of the overlying volcanic deposit (S.U. A, 378 ± 4 ka). In contrast, the isochron plot built from the teeth
348 with cement population does not allow any age determination.

349 Valle Giumentina - The $^{40}\text{Ar}/^{39}\text{Ar}$ chronology obtained for the Valle Giumentina sequence, previously supposed
350 contemporaneous with the Rissian Glacial stage (MIS 6-8, Demangeot and Radmilli, 1953), indeed covers two gla-
351 cial/interglacial cycles from MIS 15 to MIS 12 (see discussions in Nicoud et al., 2016 ; Villa et al., 2016 ; Limondin-
352 Lozouet et al., 2017). The ESR/U-series age obtained for the tooth carried out from Acheulean ALB level, 449 ± 29 ka,
353 is undistinguishable from the $^{40}\text{Ar}/^{39}\text{Ar}$ age of LABM level located just below, 455 ± 3 ka.

354 Isernia La Pineta - A primary fallout tephra layer located just below the main archaeological level t3a was dated
355 by $^{40}\text{Ar}/^{39}\text{Ar}$ of 584 ± 5 ka (Peretto et al., 2015), furnishing a maximum age for this level. The age underestimation of
356 ESR/U-series data is here more severe, around 25% (mean age) lower than this date. The hypothesis of a change of
357 the external dose in relation with late uptake history in the palaeontological remains was proposed previously to ex-
358 plain this age underestimation (Falguères et al., 2007; Shao et al., 2011), but it should be underlined that the isochron
359 age obtained for these teeth (585 ka) is in perfect agreement with the $^{40}\text{Ar}/^{39}\text{Ar}$ date .

360 Notarchirico - The situation is different at Notarchirico. For the teeth recovered from the palaeoanthropological level
361 supra α , both the ESR/US ages (ranging from 208 ± 32 ka to 546 ± 64 ka), are so scattered that it precludes any mean
362 age calculation. Isochron age estimate (134 ka) is much younger than the $^{40}\text{Ar}/^{39}\text{Ar}$ age time range estimate, dated
363 between 612 ± 4 ka and 659 ± 9 ka (Pereira et al., 2015). These results indicate that the teeth have either recently
364 experienced an event avoiding ESR/U-series dating possibilities or that the palaeodosimetric reconstruction cannot be
365 realized from present-day data. On the other hand, the ages derived from ESR analyses of Notarchirico sediments are
366 quite coherent despite the fact than only the Al center was usable. The obtained ESR age (657 ± 31 ka) agrees at 1σ
367 with the $^{40}\text{Ar}/^{39}\text{Ar}$ age estimate for this level, constrained between 658 and 612 ka.

369 Discussion

370 The main purpose of the present paper was to discuss of the chronologies established by ESR and ESR/U-series
371 methods on sediments and teeth sampled for various Middle Pleistocene sites of Central and Southern Italy, displaying
372 into their stratigraphic sequences also volcanic materials dated by $^{40}\text{Ar}/^{39}\text{Ar}$ on single grains. The figure 4 summarizes
373 the whole set of data obtained on the studied sites.

374 $^{40}\text{Ar}/^{39}\text{Ar}$ method was then used as reference method to provide independent chronological data on the studied
375 archaeological sites. $^{40}\text{Ar}/^{39}\text{Ar}$ results permit hence to place with confidence the studied sites in a single precise and
376 coherent chronological framework. The site succession from the youngest to the older is the following: La Polledrara
377 di Cecanibbio < Guado San Nicola \approx Isoletta \approx Lademagne < Valle Giumentina < Isernia la Pineta < Notarchirico. This
378 succession is slightly different than the biochronological succession previously proposed for these sites and in which
379 Isernia was supposed equivalent in age or slightly older than Notarchirico (Sardella et al., 2006; Palombo and Sardella,
380 2007; Marra et al., 2014). From the archaeological point of view, this chronology ranges the deposition of the long
381 stratigraphic sequence of Valle Giumentina from MIS 15 to MIS 12, while it was considered as coeval with the Rissian
382 Glacial stage (MIS 6-8, Demangeot and Radmilli, 1953). Moreover $^{40}\text{Ar}/^{39}\text{Ar}$ data indicate that the archaeological levels
383 of Guado San Nicola, in which Mode 3 lithic industry was recovered, are contemporaneous with the MIS 11 and 10
384 periods, placing the site among the oldest occurrences of this type of lithic technology (Peretto et al., 2014, 2016).

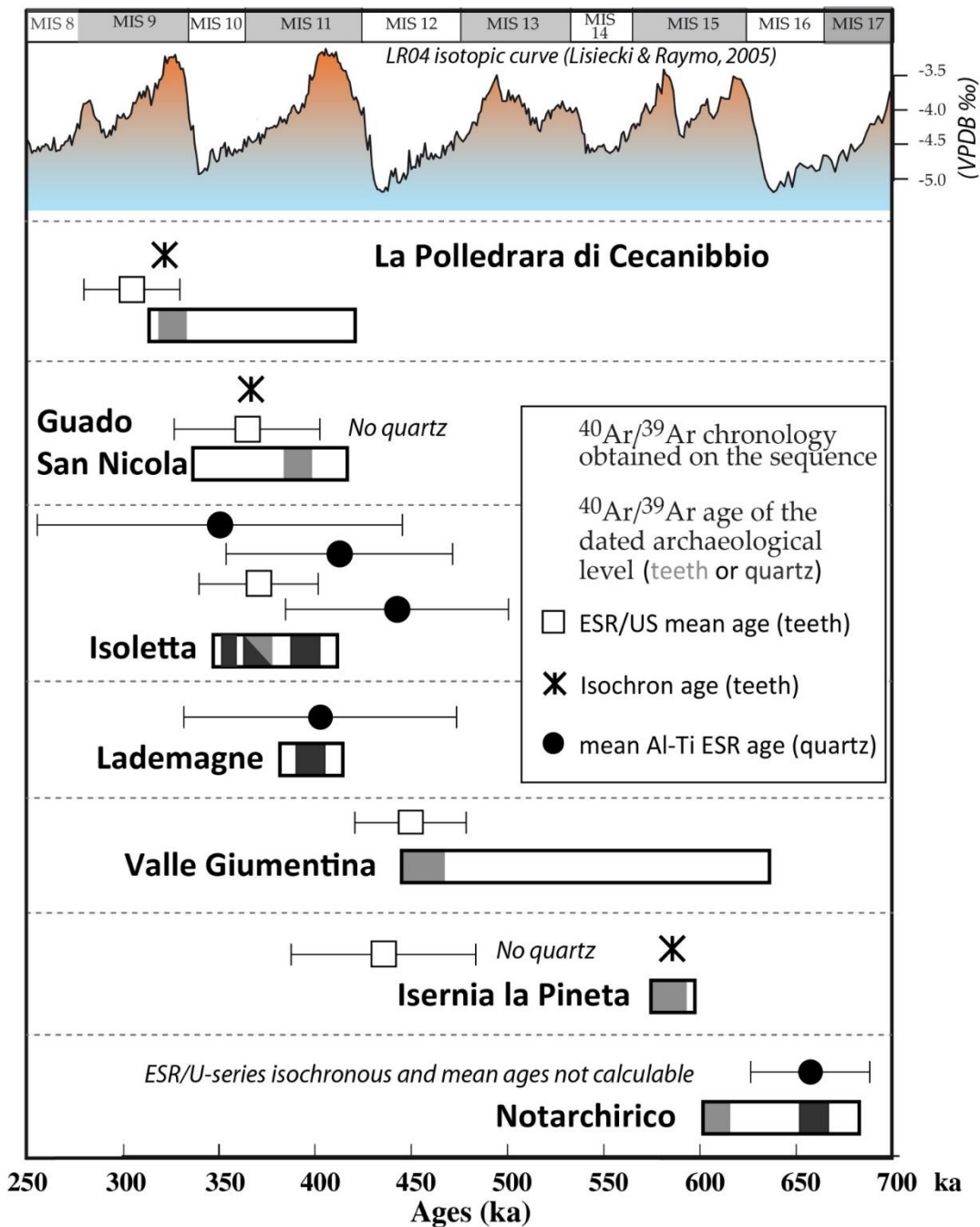


Figure 4 – ESR and ESR/U-series ages obtained for the different studied Middle Pleistocene sites of Central and Southern Italy with indication of the corresponding $^{40}\text{Ar}/^{39}\text{Ar}$ chronology.

The ESR ages obtained on the fluvial quartz grains are globally in agreement with these $^{40}\text{Ar}/^{39}\text{Ar}$ chronologies on the studied sites. The results derived from Al and Ti-Li ESR centers are globally similar for the main part of the analysed samples, while equivalent doses and ages obtained using Ti-H center are systematically underestimated, perhaps in relation with a faster saturation of these centers. Voinchet et al. (2020) recommend hence that Ti-H centers should not be used to date samples with equivalent doses greater than ca 300 Gy. These authors underline also that, if Al-center use can provide overestimated age estimate in case of incomplete initial bleaching, Ti-Li center measurement can be complicated for samples displaying poor signal-to-noise resolution (Voinchet et al., 2020).

397 On the other hand, the ages obtained from ESR/U-series results for the different studied sites in which several
398 teeth were analysed appear quite systematically underestimated. This underestimation is slight for the main part of
399 the teeth recovered from the two younger sites (< 450 ka, La Polledrara and Guado San Nicola), but more drastic for
400 the whole set of teeth carried out from the two older ones (Isernia and Notarchirico) despite very different U-uptake
401 histories (systematic late uptake at Isernia and early uptake or leaching at Notarchirico). The use of the isochron ap-
402 proach attests however of the quite good reliability of the palaeodosimetric reconstruction for these different sites
403 and the observed age underestimation could therefore be related to an underestimation of the equivalent dose. In
404 such context, it should also be underlined that the results obtained for the single teeth from Isoletta and Valle Giu-
405 mentina are in agreement with the $^{40}\text{Ar}/^{39}\text{Ar}$ ages of the dated levels.

406 An explanation advanced to explain such age underestimation could be linked to the high U contents recorded in
407 some of the analysed teeth enamels and associated high internal doses reconstruction. The possibility of an inverse
408 correlation between the uranium concentration and ESR signal intensities in enamel displaying high U content was
409 indeed postulated, considering that the crystal lattice of the enamel could locally be completely destroyed by alpha
410 radiations emitted by uranium decay and so that the measured ESR signal corresponds only to low uranium area (Ba-
411 hain et al., 1992). This assumption has however never been demonstrated and the results of the present study indicate
412 that, if such effect could exist, it cannot explain the whole set of data obtained in the present study. Indeed, the asso-
413 ciation of high U content in enamel, low D_E value and leaching evidence in the different dental tissues (corresponding
414 to high $^{230}\text{Th}/^{234}\text{U}$ ratios) leads to more or less severe age underestimation.

415 Another possible explanation of such age underestimation is linked to the fact that ESR signal of enamel is indeed
416 resulting of several CO_2^- radicals having different stabilities (Joannes Boyau and Grün, 2009). These radicals are indis-
417 tinguishable from each other when working on powders as during the present study, but can be distinguished by anal-
418 yses of enamel fragments (Joannes Boyau et al., 2010; see also discussion in Joannes Boyau, 2013 and references
419 therein). Some of these radicals are unstable considering geological time range and are considered as responsible for
420 an underestimation of up to 30% of D_E values (Joannes Boyau and Grün, 2011). The equivalent doses derived from T1-
421 B2 peak-to-peak measurements could therefore be affected by this lower stability of these unstable CO_2^- radicals to a
422 greater or lesser degree. It could be also dependant on the dose rate intensity, complicating for the moment the taking
423 into account of this parameter. Systematic comparisons between powder and enamel fragment ESR studies could al-
424 low a better estimation of the impact of this poor stability but it necessitates specific ESR equipment and is very time
425 consuming. As the isochron plots provide results in agreement for part of the studied teeth sets, it seems that an

426 reliable age estimate can be obtained by this way if the dose rate has not changed over the geological history of the
427 site in question. Here also, such assumption will have to be confirmed by subsequent studies. It could be also interest-
428 ing to rely powder and fragment studies as well to try to characterize the relative percentages of stable and unstable
429 CO_2^- radicals in ESR powder spectra to correct for each sample a possible D_E underestimation. Unfortunately, such
430 studies are still scarce and the various methods proposed to such correction were not sufficiently checked with inde-
431 pendent age control and systematic corrections seem thus to be premature (see details in Joannes Boyau, 2013).

432 Despite these questions, the results obtained in the present study are encouraging and permitted to clarify the
433 chronology of the early Middle Pleistocene prehistoric sites in Italy, ranging approximately between 300 and 700 ka.
434 We are currently trying to apply to other site the same multi-method approach associating ESR and ESR/U-series with
435 independent radiisotopic methods ($^{40}\text{Ar}/^{39}\text{Ar}$, but also U-series, ^{14}C and other cosmonuclides) s, either more recent
436 (late Middle Pleistocene and Upper Pleistocene) or older (Lower Pleistocene).

437

438 **Conclusions**

439 The ESR and combined ESR/U-series ages determined from analyses realized respectively on quartz and teeth
440 carried out from several Middle Pleistocene Italian sites were systematically compared with $^{40}\text{Ar}/^{39}\text{Ar}$ ages obtained
441 on K-feldspars minerals derived from volcanic or fluvial deposits. The ESR/U-series ages seem quite systematically
442 underestimated (from 1 to 66 % depending on the age of the sites) but the isochron age estimates obtained on three
443 sites are in agreement with the corresponding $^{40}\text{Ar}/^{39}\text{Ar}$ chronologies and indicate that the palaeodosimetric recon-
444 struction is generally correct for the dated levels, with the notable exception of Notarchirico site. For the quartz ESR
445 dating, the multi-center approach was used when possible. The ages determined both from Ti-Li and Al signals are
446 generally in agreement with each other and consistent with the $^{40}\text{Ar}/^{39}\text{Ar}$ ages, while the Ti-H age estimates appear as
447 underestimated for samples associated to D_E values higher than 300 Gy, suggesting a saturation of the Ti-H traps in
448 these samples (Voinchet et al., 2020).

449 These results are overall encouraging and pinpoints the necessity when possible to cross-check the methods as
450 well to analyse several samples by dated level. At Notarchirico, both ESR/U-series and isochron ages are much younger
451 than the expected age, by contrast with the ESR age which is in good agreement with the $^{40}\text{Ar}/^{39}\text{Ar}$ ages. Lastly, at
452 Isoletta, both ESR/U-series, ESR and $^{40}\text{Ar}/^{39}\text{Ar}$ are in good agreement. These data indicate also that the ESR/U-series
453 and ESR chronologies established on Western European Palaeolithic sites when other independent methods are not
454 available reflect rather well the geological ages of the dated Middle Pleistocene levels.

455

456 **Acknowledgements**

457 We would like to express our gratitude to the Italian archaeologists and administrative service that allowed the reali-
458 zation of this study, with special thanks to Anna-Paola Anzidei †, Marta Arzarello, Daniele Aureli, Italo Biddittu, Grazia-
459 Maria Bulgarelli Giuseppe Lembo, Brunella Muttillio, Marie-Hélène Moncel, Elisa Nicoud, Carlo Peretto, Christian Per-
460 renoud, Marcello Piperno, Benedetto Sala and Valentina Villa for their availability, patience and helpful discussions.
461 We want also thank the two anonymous reviewers for their constructive comments and suggestions that are permit-
462 ted to greatly improve the manuscript.

463 The present study was financially supported by the ATM program «Les dynamiques socio-écologiques, entre
464 perturbations et résiliences environnementales et culturelles» of the MNHN (project «Acheulean and volcanism in
465 Italy» conducted by M.-H. Moncel (CNRS) and J.-J. Bahain (MNHN)) and the PHC Galileo project no. 28237WA «l'Acheu-
466 léen en Italie méridionale: Chronologie, Paléanthropologie, Cultures» led by J.-J. Bahain (MNHN) and C. Peretto (Uni-
467 versity of Ferrara) which allowed the funding of part of the field missions. The PhD project of Alison Pereira was finan-
468 cially supported by the “Ecole Française de Rome” and the “Université Franco-Italienne”. Olivier Tombret has bene-
469 fited from the help of the French National Research Agency, LabEx ANR-10-LABX-0003-BCDiv, within the project “In-
470 vestissements d'avenir” n_ ANR-11-IDEX-0004-02.

471 The ESR and mobile gamma-ray spectrometers of the French National Museum of Natural History were bought
472 with the financial support of the ‘Sesame Île-de-France’ program, the ‘Région Centre’ and the aforementioned BcDIV
473 program respectively.

474

475

476 **References**

477 Anzidei, A.P., Arnoldus Huizendveld, A., Palombo, M.R., Argenti, P., Caloi, L., Marcolini, F., Lemorini, L., Mussi, M.,
478 2004. Nouvelles données sur le gisement Pléistocène moyen de La Polledrara di Cecanibbio (Latium, Italie). In: Baque-
479 dano, E., Rubio, S. (Eds.), Miscelánea en homenaje a Emiliano Aguirre. Zona Archeologica 4. Archeologia. Museo Ar-
480 queológico Regional, Madrid, 20-29.

481 Anzidei, A.P., Bulgarelli, G.M., Catalano, P., Cerilli E., Gallotti R., Lemorini C., Milli S., Palombo, M.R., Pantano, W.,
482 Santucci, E., 2012. Ongoing research at the late Middle Pleistocene site of La Polledrara di Cecanibbio (central Italy),
483 with emphasis on human elephant relationships. *Quaternary international* 255, 171-187.

484 Apers, D., Debuyst, R., Cannière, P. de, Dejehet, F., Lombard, E., 1981. Critique de la datation par résonance parama-
485 gnétique électronique (ESR) des planchers stalagmitiques de la Caune de l'Arago. In: Lumley, H. de, Labeyrie, J. de
486 (Ed), *Datations et Analyses Isotopiques en Préhistoire: Méthodes et Limites*. Edition du CNRS, Paris, pp. 533-550 pre-
487 print.

488 Ascenzi, A., Biddittu, I., Cassoli, P.F., Segre, A.G., Segre Naldini, E., 1996. A calvarium of late *Homo erectus* from
489 Ceprano, Italy. *Journal of Human Evolution* 31, 409-423.

490 Bahain J.-J., Shao Q., Falguères C., Garcia T., Dolo J.-M., Douville E., Frank N., 2014. Datation du site de Guado San Nicola
491 di Monteroduni par les méthodes de la résonance de spin électronique et du déséquilibre dans les familles de l'ura-
492 nium combinées (ESR/U-Th). In Muttilo B., Lembo G., Peretto C. (dir), *L'insediamento a bifacciali di Guado San Nicola*
493 (Monteroduni, Molise, Italia), *Annali dell'Università di Ferrara Museologia Scientifica e Naturalistica*, 10/1, 53-56

494 Bahain J.-J., Falguères C., Dolo J.-M., Antoine P., Auguste P., Limondin-Lozouet, N., Lochet J.-L., Tuffreau A., 2010. ESR/U-
495 series dating of teeth recovered from well-stratigraphically age-controlled sequences from Northern France. *Quater-
496 nary Geochronology* 5, 371-375.

497 Bahain, J.-J., Yokoyama, Y., Falguères, C., Sarcia, M.N., 1992. ESR dating of tooth enamel: a comparison with K-Ar da-
498 ting. *Quaternary Science reviews*, 11, 245-250.

499 Biddittu, I., 2004. *Guida del Museo Preistorico di Pofi*. I Quad. di ARGIL 1, 1-158.

500 Biddittu, I., Canetri, E., Comerci, V., Germani, M., Picchi, G., 2012. Nuove ricerche nel giacimento del Paleolitico infe-
501 riore di Lademagne, S. Giovanni Incarico (Frosinone). In Ghini, G. and Mari, Z., (eds) *Lazio e Sabina*, Edizioni Quasar, 9,
502 437-443.

503 Bischoff J.L., Robert J., Rosenbauer R.J.V., 1988. A test of Uranium-series dating of fossil tooth enamel: result from
504 Tournal Cave, France. *Applied Geochemistry* 3, 145-151.

505 Blackwell, B.A., Schwarcz, H.P., 1993. ESR isochron dating for teeth: a brief demonstration in solving the external dose
506 calculation problem. *Applied Radiation and Isotopes* 44, 243-252.

507 Brennan, B, Lyons, R, Phillips, S. 1991. Attenuation of alpha particle track dose for spherical grains. Nuclear Tracks
508 Radiation Measurements 18, 249-253.

509 Brennan, B. 2003. Beta doses to spherical grains. Radiation Measurements 37, 299- 303.

510 Brennan, B.J., Rink, W.J., McGuirl, E.L., Schwarcz, H.P., Prestwich, W.V., 1997. Beta doses in tooth enamel by “One
511 Group” theory and the Rosy ESR dating software. Radiation Measurements 27, 307–314.

512 Brown F.H., McDougall I., Gathogo P.N., 2012. Age ranges of Australopithecus species, Kenya, Ethiopia and Tanzania.
513 In Reed K.E., Fleagle J.G., Leakey R. (eds.) The Paleobiology of Australopithecus, Vertebrate Paleobiology and Paleoan-
514 thropology Series, Springer, PP 7-20.

515 Coltorti M, Cremaschi M, Delitalia MC, Esu D, Fornaseri M, McPherron A, Nicoletti M., Van Otterloo R., Peretto C., Sala
516 B., Schmidt V., Sevink J. 1982. Reversed magnetic polarity at an early Lower Palaeolithic site in central Italy. Nature
517 300, 173–176

518 Dolo J.M., Lecerf N., Mihajlovic V., Falguères C., Bahain J.-J., 1996. Contribution of ESR dosimetry for irradiation of
519 geological and archaeological samples with a ⁶⁰Co panoramic source. Applied Radiation and Isotopes 47, 1419-1421

520 Duval M., Grün R., Falguères C., Bahain J.-J., Dolo J.-M., 2009. ESR dating of Lower Pleistocene fossil teeth: limits of the
521 single saturating exponential (SSE) function for the equivalent dose determination. Radiation measurements 44, 477-
522 482.

523 Duval, M. Grün, R., 2016. Are published ESR dose assessments on fossil tooth enamel reliable? Quaternary Geochro-
524 nology 31, 19-27.

525 Duval, M., Guilarte, V., 2015. ESR dosimetry of optically bleached quartz grains extracted from Plio-quaternary sedi-
526 ment: evaluating some key aspects of the ESR signal associated to the Ti-center. Radiation Measurement 78, 28–41

527 Falguères, C., Bahain, J.-J., Dolo, J.-M., Mercier, N. , Valladas, H., 2007. On the interest and the limits of using combined
528 ESR/U-series model in the case of very late uranium uptake. Quaternary Geochronology 2, 403–408.

529 Grün, R., 1994. A cautionary note: use of the “water content” and “depth for cosmic ray dose rate” in AGE and DATA.
530 Ancient TL 12, 50- 51.

531 Grün, R., 2000. Methods of dose determination using ESR spectra of tooth enamel. Radiation Measurements 32, 767-
532 772

533 Grün, R., Katzenberger-Apel, O., 1994. An alpha irradiator for ESR dating. *Ancient TL* 12, 35–38.

534 Grün, R., Schwarcz, H.P., Chadam, J.M., 1988. ESR dating of tooth enamel: coupled correction for U-uptake and U-
535 series disequilibrium. *Nuclear Tracks and Radiation Measurements*, 14, 237-241.

536 Guérin, G., Mercier, N., Adamiec, G., 2011. Dose-rate conversion factors: update. *Ancient TL*, 29, 5-8.

537 Joannes-Boyau R., 2013. Detailed protocol for an accurate non-destructive direct dating of tooth enamel fragment
538 using electron spin resonance. *Geochronometria* 40, 322-333.

539 Joannes-Boyau R., Grün R., 2009. Thermal behavior of oriented and non-oriented CO₂- radicals in tooth enamel. *Radi-
540 ation Measurements* 44, 505-511.

541 Joannes-Boyau R., Bodin T., Grün R., 2010. Decomposition of the angular ESR spectra of fossil tooth enamel fragments.
542 *Radiation Measurements* 45, 887-898.

543 Joannes-Boyau R., Grün R., 2011. A comprehensive model for CO₂- radicals in fossil tooth enamel: implications for ESR
544 dating. *Quaternary Geochronology* 6, 82-97.

545 Laurent, M., Falguères, C., Bahain, J.-J., Rousseau, L., Van Vliet-Lanoë, B. 1998. ESR dating of quartz extracted from
546 Quaternary and Neogene sediments: method, potential and actual limits. *Quaternary Science Reviews* 17, 1057-1061.

547 Lee, J.Y., Marti, K., Severinghaus, J.P., Kawamura, K., Hee-Soo, Y., Lee, J.B., Kim, J.S., 2006. A redetermination of the
548 isotopic abundances of atmospheric Ar. *Geochimica et Cosmochimica Acta* 70, 4507-4512

549 Lefèvre D., Raynal J.-P., Vernet G., Kieffer G., Piperno M., 2010. Tephro-stratigraphy and the age of ancient Southern
550 Italian Acheulean settlements: The sites of Loreto and Notarchirico (Venosa, Basilicata, Italy). *Quaternary International*
551 223–224, 360–368

552 Limondin-Lozouet N., Villa V., Pereira A., Nomade S., Bahain J.-J., Stoetzel E., Aureli D., Nicoud E., 2017. Middle Pleis-
553 tocene molluscan fauna from Central Italy at Valle Giumentina (Abruzzo): palaeoenvironmental, biostratigraphical and
554 biogeographical implications. *Quaternary Science Reviews* 156, 135-149

555 Lisiecki, L.E., Raymo, M.E. 2005. A Pliocene-Pleistocene stack of 57 globally distributed benthic δ¹⁸O records.
556 *Paleoceanography* 20, PA 1003, doi:10.1029/2004PA001071

557 Ludwig K. R., 2003. Isoplot 3.0, a geochronological toolkit for Microsoft Excel. *Berkeley Geochronology Center Special
558 Publication*, 4, 71p

559 McDougall I., 2014. K/Ar and $^{40}\text{Ar}/^{39}\text{Ar}$ isotopic dating techniques as applied to young volcanic rocks, particularly
560 those associated with hominin localities. In Holland H.D., Turekian K.K. (eds) *Treatise on Geochemistry*, 14, 1-15

561 Mallegni F., Segre A.G., Segre-Naldini E., 1991. Découverte d'un fémur acheuléen à Notarchirico (Venosa, Basilicate).
562 *L'Anthropologie* 95, 47-88.

563 Manzi, G. 2016. Humans of the Middle Pleistocene: The controversial calvarium from Ceprano (Italy) and its signifi-
564 cance for the origin and variability of *Homo heidelbergensis*. *Quaternary International* 411, 254-261.

565 Marra F., Pandolfi L., Petronio C., Di Stefano G., Gaeta M., Salari L., 2014. Reassessing the sedimentary deposits and
566 vertebrate assemblages from Ponte Galeria area (Rome, central Italy): An archive for the Middle Pleistocene faunas of
567 Europe. *Earth-Science Reviews* 139, 104–122.

568 Marra, F., Nomade, S., Pereira, A., Petronio, C., Salari, L., Sottili, G., Bahain, J.J., Boschian, G., Di Stefano, G., Falguères,
569 C., Florindo, F., Gaeta, M., Giaccio, B., Masotta, M., 2018. A review of the geologic sections and the faunal assemblages
570 of Aurelian Mammal Age of Latium (Italy) in the light of a new chronostrati-graphic framework. *Quaternary Science*
571 *Reviews* 181, 173–199.

572 Murray, A.S., Roberts, R.G., 1997. Determining the burial time of single grains of quartz using optically stimulated
573 luminescence. *Earth and Planetary Science Letters* 152, 163-180.

574 Niespolo, E.M., Rutte, D., Deino, A., Renne, P.R., 2017. Intercalibration and age of the Alder Creek sanidine $^{40}\text{Ar}/^{39}\text{Ar}$
575 standard. *Quaternary Geochronology* 39, 205-213.

576 Nomade, S., Gauthier, A., Guillou, H., Pastre, J.F., 2010. $^{40}\text{Ar}/^{39}\text{Ar}$ temporal framework for the Alleret maar lacus-
577 trine sequence (French Massif Central): Volcanological and Paleoclimatic implications. *Quaternary Geochronology* 5,
578 20-27.

579 Nomade, S., Renne, P.R., Vogel, N., Deino, A.L., Sharp, W.D., Becker, T.A., Jaouni, A.R., Mundil, R., 2005. Alder Creek
580 sanidine (ACs-2), A Quaternary $^{40}\text{Ar}/^{39}\text{Ar}$ dating standard tied to the Cobb Mountain geomagnetic event. *Chemical*
581 *Geology* 218, 315–338.

582 Palombo M.R., Sardella R., 2007. Biochronology and biochron boundaries: A real dilemma or a false problem? An ex-
583 ample based on the Pleistocene large mammalian faunas from Italy *Quaternary International* 160, 30–42.

584 Pereira A., Nomade S., Falguères C., Bahain J.-J., Tombret O., Garcia T., Voinchet P., Bulgarelli G.-M., Anzidei A.-P.,
585 2017. New $^{40}\text{Ar}/^{39}\text{Ar}$ and ESR/U-series data for the La Polledrara di Cecanibbio archaeological site (Lazio, Italy). *Journal*
586 *of Archaeological Science: Reports* 15, 20-29.

587 Pereira A., Nomade S., Moncel M.-H., Voinchet P., Bahain J.-J., Biddittu I., Falguères C., Giaccio B., Manzi G., Parenti
588 F., Scardia G., Scao V., Sottili G., Vietti A. , 2018. Integrated geochronology of Acheulian sites from the southern La-
589 tium (central Italy): Insights on human-environment interaction and the technological innovations during the MIS 11-
590 MIS 10 period. *Quaternary Science Reviews* 187, 112-129.

591 Pereira A., Nomade S., Shao Q., Bahain J.-J., Arzarello M., Douville E., Falguères C., Frank N., Garcia T., Lembo G.,
592 Muttillio B., Peretto C., 2016. $^{40}\text{Ar}/^{39}\text{Ar}$ and ESR-U/Th dates for Guado San Nicola, Middle Pleistocene key site at the
593 Lower/Middle Palaeolithic transition in Italy. *Quaternary Geochronology*, 36, 67-75

594 Pereira A., Nomade S., Voinchet P., Bahain J.-J., Falguères C., Garon H., Lefèvre D., Raynal J.-P., Scao V., Piperno M.,
595 2015. The earliest securely dated hominid fossil in Italy and evidences of Acheulian human occupations during glacial
596 MIS 16 at Notarchirico (Venosa, Basilicata, Italy). *Journal of Quaternary Science*, 30 (7), 639-650

597 Peretto C., Arnaud J., Moggi-Cecchi J., Manzi G., Nomade S., Pereira A., Falguères C., Bahain J.-J., Grimaud-Hervé D.,
598 Berto C., Sala B., Lembo G., Muttillio B., Gallotti R., Thun Hohenstein U., Vaccaro C., Coltorti M., Arzarello M., 2015. A
599 Human Deciduous Tooth and New $^{40}\text{Ar}/^{39}\text{Ar}$ Dating Results from the Middle Pleistocene Archaeological Site of Isernia
600 La Pineta, Southern Italy. *PLoS ONE*, 10 (10), e0140091

601 Peretto C., Arzarello M., Bahain J.-J., Boulbes N., Coltorti M., Dolo J.-M., Douville E., Falguères C., Frank N., Garcia T.,
602 Lembo G., Moigne A.-M., Muttillio B., Nomade S., Shao Q., Pereira A., Pieruccini P., Rufo M.A., Sala B., Thun Hohenstein
603 U., Tessari U., Turrini M.C., Vaccaro C., 2016. The Middle Pleistocene site of Guado San Nicola (Monteroduni, Central
604 Italy) on the Lower/Middle Palaeolithic transition. *Quaternary International* 411, 301-315

605 Peretto C., Terzani C., Cremaschi M., 1983. Isernia la Pineta : un accampamento piu antico di 700.000 anni. Calderine
606 editore, Bologne.

607 Peretto, C., Arzarello, M., Bahain, J.J., Boulbes, Coltorti, M., De Bonis, A., N., Douville, E., Falguères, C., Frank, N., Garcia,
608 T., Lembo, G., Moigne, Morra, V., A.M., Muttillio, B., Nomade, S., Shao, Q., Perrotta, A., Pieruccini, P., Rufo, M., Sala,
609 B., Scarpati, C., Thun Hohenstein, U., Tessari, U., Turrini, M.C., Vaccaro, C. 2014. L'occupazione umana del Pleistocene

610 medio di Guado San Nicola (Monteroduni, Molise). *Annali dell'Università di Ferrara, Museologia Scientifica e*
611 *Naturalistica* 10, 23-31.

612 Petronio C., Di Stefano G., Kotsakis T., Salari L., Marra F., Jicha B.R., 2019. Biochronological framework for the late
613 Galerian and early-middle Aurelian Mammal Ages of peninsular Italy. *Geobios*, 53, 35–50 .

614 Piperno M. 1997. Notarchirico, un sito del Pleistocene medio iniziale nel bacino di Venosa, Osanna Venosa (eds), Ve-
615 nosa.

616 Prescott, J.R., Hutton, J.T., 1994. Cosmic ray contributions to dose rates for luminescence and ESR dating: large depths
617 and long-term time variations. *Radiation Measurements*, 23, 497–500.

618 Renne, P.R., Mundil, R., Balco, G., Min, K., Ludwig, K.R., 2011. Response to the comment by W.H. Schwarz et al. on
619 “Joint determination of $40K$ decay constants and $40Ar^*/40K$ for the Fish Canyon sanidine standard, and improved
620 accuracy for $40Ar/39Ar$ geochronology” by P.R. Renne et al. (2010). *Geochimica Cosmochimica Acta* 75, 5097-5100

621 Santucci, E., Marano, F., Cerilli, E., Fiore, I., Lemorini, C., Palombo, M.R., Anzidei, A.P., Bulgarelli, G.M., 2016. *Palae-*
622 *oloxodon* exploitation at the Middle Pleistocene site of La Polledrara di Cecanibbio (Rome, Italy). *Quaternary*
623 *international* 406 part B, 169-182. .

624 Sardella R., Palombo M.R., Petronio C., Bedetti C., Pavia M., 2006. The early Middle Pleistocene large mammal faunas
625 of Italy: An overview. *Quaternary International* 149, 104–109.

626 Shao, Q., Bahain, J.-J., Falguères, C., Peretto, C., Arzarello, M., Minelli, A., Hohenstein, U.T., Dolo, J.-M., Garcia, T.,
627 Frank, N., Douville, E., 2011. New ESR/U-series data for the early middle Pleistocene site of Isernia la Pineta, Italy.
628 *Radiation Measurements* 46, 847-852.

629 Shao, Q., Bahain, J.-J., Falguères, C., Dolo, J.-M., Garcia, T., 2012. A new U-uptake model for combined ESR/U-series
630 dating of tooth enamel. *Quaternary Geochronology*, 10, 406-411.

631 Shao, Q., Bahain, J.-J., Dolo, J.M., Falguères, C., 2014. Monte Carlo approach to calculate US-ESR ages and their uncer-
632 tainties. *Quaternary Geochronology* 22, 99-106.

633 Shao Q., Bahain J.-J., Wang W., Jin C., Wang Y., Voinchet P., Lin M., 2015a. Combined ESR and U-series dating of early
634 Pleistocene *Gigantopithecus* faunas at Mohui and Sanhe Caves, Guangxi, southern China. *Quaternary Geochronology*,
635 30, 524-528

636 Shao Q., Chadam J., Grün R., Falguères C., Dolo J.-M., Bahain J.-J., 2015b. The mathematical basis for the US-ESR dating
637 method. *Quaternary Geochronology* 30, 1-8

638 Steiger, R.H., Jäger, E., 1977. Subcommission on geochronology: convention on the use of decay constants in geo- and
639 cosmochronology. *Earth and Planetary Science Letters* 6, 359-362.

640 Tissoux, H., Voinchet, P., Lacquement, F., Prognon, F., Moreno, D., Falguères, C., Bahain, J.-J., Toyoda S. 2013. Investi-
641 gation on non-optically bleachable components of ESR aluminium signal in quartz. *Radiation Measurements*, 47, 9,
642 894-899.

643 Toyoda, S., Voinchet, P., Falguères, C., Dolo, J.M., Laurent, M., 2000. Bleaching of ESR signal by the sunlight: a labora-
644 tory experiment for establishing the ESR dating of sediments. *Applied Radiation Isotopes*, 52, 5, 1357–1362.

645 Toyoda, S., Falguères C., 2003. The method to represent the ESR signal intensity of the aluminium hole center in quartz
646 for the purpose of dating. *Advances in ESR applications*, 20, 7-10.

647 Vandenbergue, D., De Corte, F., Buylaert J.P., Kucera, J., Van den haute, P., 2008. On the internal radioactivity in quartz.
648 *Radiation Measurements* 43, 771-775.

649 Voinchet, P., Bahain, J.J., Falguères, C., Laurent, M., Dolo, J.M., Despriée, J., Gageonnet, R., Chaussé, C., 2004. ESR
650 dating of Quartz extracted from Quaternary sediments: application to fluvial terraces system of Northern France. *Qua-
651 ternaire* 15, 135-142.

652 Voinchet, P., Yin, G., Falguères, C., Liu, C., Fei, H., Sun, X., Bahain, J.J., 2013. ESR dose response of the Al center meas-
653 ured in quartz samples from the Yellow River (China): implications for the dating of Upper Pleistocene sediment.
654 *Geochronometria* 40, 341–347.

655 Voinchet, P., Pereira, A., Nomade, S., Falguères, C., Biddittu, I., Piperno, M., Moncel, M.-H., Bahain, J.-J., 2020. ESR
656 dating applied to optically bleached quartz - a comparison with $^{40}\text{Ar}/^{39}\text{Ar}$ chronologies on Italian Middle Pleistocene
657 sequences, *Quaternary International*, 556, 113-123 .

658 Yokoyama, Y., Falguères, C., Quaegebeur, J.P., 1985. ESR dating of quartz from Quaternary sediments: first attempts.
659 *Nuclear Tracks* 10, 921-928.

660

661

662 **Figure caption**

663

664 **Figure 1** - Location of the studied Middle Pleistocene sites in Central and Southern Italy.

665

666 **Figure 2** – Simplified stratigraphic logs of the studied Middle Pleistocene sites with indication of the levels dated by
667 $^{40}\text{Ar}/^{39}\text{Ar}$ and positions of the levels sampled for ESR and ESR/U-series studies. $^{40}\text{Ar}/^{39}\text{Ar}$ ages were obtained directly
668 on tephra levels (primary deposits) or on potassic feldspar grains extracted from fluvial sediments (secondary
669 deposits), the youngest population corresponding then to a maximum age for the dated level.

670

671 **Figure 3** – Age density probability plots (left, built using Isoplot 3.0 software, Ludwig, 2003) and isochron plots (right)
672 obtained for the different studied Middle Pleistocene sites of Central and Southern Italy with indication of the corre-
673 sponding $^{40}\text{Ar}/^{39}\text{Ar}$ chronology. The U-uptake accumulated dose corresponds to the sum of the internal (enamel) and
674 beta dose (corresponding to dentine and eventually cement) reconstructed for the considered sample all along its
675 geological history from the modelled uptake parameters.

676

677 **Figure 4** – ESR and ESR/U-series ages obtained for the different studied Middle Pleistocene sites of Central and South-
678 ern Italy with indication of the corresponding $^{40}\text{Ar}/^{39}\text{Ar}$ chronology.

679

680 **Table caption**

681

682 **Table 1** – List and nature of the analysed teeth from several Middle Pleistocene Italian sites

683

684 **Table 2** – $^{40}\text{Ar}/^{39}\text{Ar}$ ages obtained from volcanic minerals recovered from several Middle Pleistocene Italian sites.

685 The indicated $^{40}\text{Ar}/^{39}\text{Ar}$ age corresponds to the age of the youngest homogeneous potassic feldspars population.

686 These ages were re-calculated in the present contribution according to the monitor flux standard ACs-2 at 1.1891 Ma

687 (Niespolo e al., 2017) and the K total decay constant of Renne et al. (2011) from the original data published in the

688 various referred papers. A homogeneous population is considered relevant when the weighted mean of these crystals has the following statistical characteristics: MSWD < 1.5, Probability fit ≥ 0.1 . The weighted average ages were
689 calculated using IsoPlot 3.0 (Ludwig, 2003) and given at 95% (2σ) of confidence.
690

691
692 **Table 3** – ESR data and ages for sediments recovered from several Middle Pleistocene Italian sites.

693 Equivalent doses (D_E) were derived from the obtained intensity growth curves using an exponential + linear function
694 for Al and Ti-Li centers (Duval et al., 2009; Voinchet et al., 2013) and by a single saturating exponential function for Ti-
695 H from the six first points of the growth curves (Voinchet et al., 2020) with Microcal OriginPro 8 software, both with
696 $1/I^2$ weighting (according with Yokoyama et al., 1985). Age calculations were performed using the following parameters:
697 dose-rate conversions factors from Guérin et al. (2011); a k-value of 0.15 ± 0.1 (Laurent et al., 1998); alpha and
698 beta attenuations from Brennan (2003) and Brennan et al. (1991); water attenuation formulae from Grün (1994);
699 cosmic dose rate estimated from the Prescott and Hutton's equations (1994). The internal dose rate was considered
700 as negligible because of the low contents of radionuclides usually found in quartz grains (Murray and Roberts 1997;
701 Vandenbergue et al. 2008). ESR age estimates are given with one sigma error range.
702

703 **Table 4** – U-series and ESR data for the analysed teeth recovered from several Middle Pleistocene Italian sites.

704 U-series analyses were performed on each dental tissue in order to determine the U-uptake parameters necessary to
705 the dose rate contributions and age calculations (see details in Shao et al., 2015b), either by alpha spectrometry
706 (MNHN, Paris), or by Neptune Multi-Collector Inductively Coupled Plasma Mass Spectrometer (MC-ICPMS) (Nanjing
707 Normal University, China).
708

709 **Table 5** – ESR/U-series data and ages for the analysed teeth recovered from several Middle Pleistocene Italian sites.

710 The equivalent doses D_E were extrapolated from the obtained dose-response data sets using either The growth curves
711 were built for each sample using different fitting functions (single saturating exponential, SSE, according with Apers et
712 al., 1981; double saturating exponential function (DSE), according with Duval et al. (2009), or exponential plus linear
713 function (E+L), according with Shao et al. (2015a). The equivalent dose corresponding to the function that best describes
714 the experimental data and gives the best statistics is then used to calculate age.

715 The radioelement contents of sediment samples associated to each tooth were determined by in laboratory high res-
716 olution low background gamma spectrometry and *in situ* gamma measurements with TL Al₂O₃ dosimeters at La
717 Polledrara and Inspector 1000 Canberra gamma spectrometer on the other sites. A sediment water content value of
718 15 ± 5 % was therefore assumed for the age calculations. The cosmic dose rate was estimated using the formula of
719 Prescott and Hutton (1994). Were also used the following parameters: a k-value (α efficiency) of 0.13 ± 0.02 (Grün and
720 Katzenberger-Apel, 1994); water content of 0 wt% in the enamel and 7 wt% in the dentine and cementum; conversion
721 contents-doses factors from Guérin et al.; (2011). For each dental tissue, Rn loss was estimated from both gamma and
722 alpha/ICP measurements (Bahain et al., 1992). The beta dose contributions were corrected from the enamel part de-
723 stroyed on each side of the enamel layer during the preparation process (according to Brennan et al., 1997).

724 ESR/U-series ages, different dose-rate contributions and U-uptake parameters were then calculated using either
725 US model (Grün et al., 1988) or AU model (Shao et al., 2012). The “USESR”, “AUESR” and “combined ESR” computer
726 programs were used for the age calculation in which the age uncertainty (1σ) is calculated with Monte Carlo approach
727 (Shao et al., 2014).

728 Isochron age estimates were newly determined in the present work except for La Polledrara samples (Pereira et al., 2017).

729